Article

Revealing Heavy Metal-Resistant Mechanisms and Bioremediation Potential in a Novel *Croceicoccus* Species Using Microbial-Induced Carbonate Precipitation

Xuya Lv [1,2], Yingwen Zhong [2], Geyi Fu [2], Yuehong Wu [1,2,*] and Xuewei Xu [1,2,*]

1   Ocean College, Zhejiang University, Zhoushan 316021, China; lvxuya@163.com
2   Key Laboratory of Marine Ecosystem Dynamics, Ministry of Natural Resources and Second Institute of Oceanography, Ministry of Natural Resources, Hangzhou 310012, China; zhongyingwen@sjtu.edu.cn (Y.Z.); fugy@sio.org.cn (G.F.)
*   Correspondence: yuehongwu@sio.org.cn (Y.W.); xuxw@sio.org.cn (X.X.)

Abstract: Polymetallic nodules and polymetallic sulfides are currently the major mineral resources found on the seabed. The motivation behind deep-sea mining arises from the pursuit of valuable metals, driven by both economic and geopolitical considerations. However, before mining can be authorized, it is crucial to understand the microbial adaptation and biomineralization process related to heavy metals in deep-sea environments. To search for potential candidate materials for bioremediation in deep-sea environment, two strains with high resistance to manganese and the ability to form rhodochrosite precipitates were isolated from the deep-sea polymetallic nodule areas and hydrothermal polymetallic sulfide areas. Genomic analysis revealed that the strains employed various effective survival strategies, such as motility, chemotaxis, biofilm formation, metal redox, and transporters, to adapt to heavy metal environments. The bacterial strains Ery5 and Ery15 promote the formation of carbonate crystals by creating an excessively alkaline environment and releasing extracellular polymeric substances (EPSs). Furthermore, strains Ery5 and Ery15 were identified using polyphasic taxonomy methods and proposed as a new species belonging to the genus *Croceicoccus*. This study presents potential candidates for bioremediation in deep-sea environments.

Keywords: heavy metal resistance; microbial-induced carbonate precipitation; *Croceicoccus*; novel species; bioremediation potential

1. Introduction

Polymetallic nodules and polymetallic sulfides are currently the main mineral resources found on the seabed. Deep-sea polymetallic nodules are known for their abundance of valuable metals, such as manganese (Mn), nickel (Ni), copper (Cu), and cobalt (Co) [1]. Among these, the CCZ (Clarion–Clipperton Zone) has the highest manganese content in its polymetallic nodules [2]. Manganese content in polymetallic nodules can be as high as 23.9% [3]. Polymetallic sulfides rich in metals, such as copper, zinc, gold, and/or silver, are deposited on the ocean crust due to hydrothermal reactions [4].

Deep-sea mining has been driven by the desire for critical metals due to their commercial and strategic significance. So far, the International Seabed Authority (ISA) has issued a total of 31 contracts for deep-sea mineral exploration. As a result, the international seabed resources are now moving from the initial exploration phase to the subsequent development phase. However, mining has significant environmental impacts, as it disrupts the ecosystem and alters the physical and chemical conditions [5]. One of the consequences is the disturbance of the fragile chemical environment at the sediment–water interface. Metal ions concentration in the interstitial water differs from that in the free water above the sediment, and mining will lead to their mixing into the bottom water. The process of

ore crushing and hydraulic transportation may cause heavy metals to leach into surrounding seawater. The discharge of mining tailings can also have an impact on the chemical environment of the water layer where they are released. No matter the mining technique employed, the process of restoration may take many years or even centuries [5]. While ISA contractors prioritize the environmental impact assessment, there is a lack of reports on the environmental restoration of deep-sea mining.

There exists a diverse range of processes and treatments accessible for reducing or recovering heavy metals from polluted soil and terrestrial water environments [6]. However, it is important to note that these processes and treatments reported so far are not applicable in deep-sea environments due to their unique characteristics. To date, there have been a few reports of manganese-resistant bacteria found in deep-sea environments (depth $\geq$ 1000 m). In addition, no microbial-induced rhodochrosite precipitation formation has been reported in the deep-sea environment until now. Thus, it has been hypothesized that bacteria originating from the in situ deep-sea environment, exhibiting heavy metal resistance and possessing the capacity for biomineralization function, could serve as promising potential candidates for bioremediation purposes. This was due to their possession of mechanisms that enable them to tolerate and adapt to the deep-sea environment. Therefore, before mining can be authorized, it is important to understand the microbial adaptation and biomineralization of heavy metal in deep-sea environments. In deep-sea polymetallic nodule areas and polymetallic sulfide areas, the distinct physical, chemical, geological, and geographical environmental conditions have created a wide variety of microbial groups with diverse metabolic types. Microorganisms inhabiting these two unique environments are challenged by excess heavy metals. Therefore, it is highly likely that these specific habitats harbor distinct microorganisms with the capability to tolerate high levels of heavy metals or are closely associated with the biogeochemical cycling of metals. These microorganisms exhibit significant potential for bio-mining valuable heavy metals and remediating environments contaminated by such elements.

After deep-sea mining, microbial-induced carbonate precipitation (MICP) is considered a potential bioremediation approach [7]. MICP is a biotechnological approach that exploits the metabolic activity of microorganisms to induce CO_3^{2-} release, thereby facilitating the sequestration of free metal ions via carbonate precipitation [8]. MICP can prevent the diffusion and migration of heavy metals. Extracellular polymeric substances (EPSs) secreted by microorganisms are rich in acidic functional groups that can bind metallic cations, accumulate metal ions, and reduce their bioavailability. Urea hydrolysis could usually accelerate the MICP process, and ureolytic bacteria are one of the common mineralizing bacteria [9]. The application of the MICP technology to Ca, Cd, Zn, Ni, Pb, and Cu immobilization has been widely investigated [10,11]. Rhodochrosite ($MnCO_3$) precipitation induced by microorganisms was only reported by *Sporosarcina pasteurii* via the decomposition of urea into ammonia and carbonates [12].

The genus *Croceicoccus* belongs to the family *Erythrobacteraceae* in the phylum *Proteobacteria*. At the moment of composing, the genus *Croceicoccus* consists of ten species, which all are isolated in marine settings, such as sediment, seawater, and biofilm that grows on the surface of boat shells [13–15]. Members of *Croceicoccus* play important roles in the deep-sea biogeochemical carbon cycle. It has been reported that *Croceicoccus marinus* E4A9[T] isolated from a polymetallic nodule area encodes a variety of esterases and glycosidases [16], and their metabolic pathways provide clues reflecting its adaptations to the ambient environment [17]. As far as we know, only *Croceicoccus naphthovorans* PQ-2[T] has been reported to have the resistance of Cr [18]. Few studies have focused on their heavy metal resistant ability and adaptation mechanisms in heavy metal environments.

In the investigation of the heavy metal-resistant bacterial diversity of deep-sea polymetallic nodule areas and hydrothermal polymetallic sulfide areas, we obtained two strains, Ery5 and Ery15, with heavy metal resistance and rhodochrosite precipitation formation. According to the analysis of the 16S rRNA gene sequence, it can be inferred that these two strains may potentially represent a novel species within the *Croceicoccus* genus. In order

to understand the mechanism of the heavy metal tolerance and biomineralization potential, this study employed genomic analysis to elucidate a diverse array of adaptive strategies towards heavy metals and provide insights into the mechanistic aspects of biomineralization. Strains Ery5 and Ery15 were identified by polyphasic taxonomy methods and proposed as a new species belonging to the genus *Croceicoccus*. This work will provide potential candidates for bioremediation in deep-sea environments.

2. Materials and Methods

2.1. Strain Isolation and Culture Conditions

Sediment samples were collected from deep-sea polymetallic nodule areas and hydrothermal polymetallic sulfide areas (Figure S1). On board the research vessel, samples were subsampled aseptically. These subsamples were then subjected to the cultural process immediately. A sediment subsample (approximately 0.1 g) was mixed in 3 mL sterile seawater and subjected to vortexing for a duration of 15 min. The mixture was spread on a medium containing different concentrations of metal ions for ten days of aerobic incubation at room temperature (about 25–28 °C). Colonies were picked and streaked for pure culture.

The strain Ery5^T was isolated from sediment collected from the Clarion–Clipperton Zone of the polymetallic nodule region of the East Pacific Ocean (154°48′ W, 09°12′ N) at a depth of 5377 m. The sample was collected via a television multicore operated from the vessel *HAI YANG LIU HAO* in September 2013. The television image revealed that over 50% of the seafloor surface was covered with abundant polymetallic nodules [19]. The isolation process involved using an LB medium supplemented with 20 mM Mn^{2+} and 30 g/L NaCl.

The strain Ery15^T was isolated from deep-sea sediment collected from South Atlantic Rise (13°20′34″ W, 21°11′7″ S) at a depth of 2687 m. The sample was collected from a television grab bucket operated from the vessel *DA YANG YI HAO* in March 2011. It was speculated that the sediment sample may be influenced by hydrothermal fluids. The isolation process involved using natural seawater agar, which was enhanced with 0.5% peptone (*w/v*; BD Difco^{TM}, Chicago, IL, USA) and 0.1% yeast extract (*w/v*; BD Difco^{TM}, Chicago, IL, USA).

2.2. Resistance and Removal Ability to Mn^{2+}

The resistance abilities of the two strains to Mn^{2+} were evaluated in an MB medium supplemented with 0–55 mM MnCl$_2$. These cultures were cultivated under constant agitation (150 rpm) at a temperature of 30 °C, and the growth was monitored by UV-visible spectrophotometry at a wavelength of 600 nm with an interval of 4 h. A parallel test was also performed with the addition of 2% urea in MB.

The Mn concentration was determined using an Inductively Coupled Plasma–Optical Emission Spectrometer (ICP-OES) (Icap Pro X, Worcester, MA, USA). Samples were filtered through a 0.22-micron filter membrane to remove residues and bacteria. The removal efficiency of manganese ions was calculated according to the equation $E = \frac{(C0 - Ct)}{C0} \times 100\%$, where E is the heavy metal removal efficiency and $C0$ and Ct represent the initial concentration and the final ultimate concentration of Mn^{2+}, respectively [20]. The experiments were conducted in triplicate to ensure accuracy, and mean ± standard deviation was reported for each measurement.

2.3. Synthesis and Characterization of Microbial-Induced Rhodochrosite

The rhodochrosite formation was tested in a marine broth (MB) medium with 20 mM MnCl$_2$ at 30 °C at 160 rpm. The visible precipitates adhering to the test tube wall and settling at the bottom of the test tube were formed after 7 days of incubation. The precipitates attaching to the wall of the test tube were scraped by tips. The precipitates were separated by natural settlement, and the liquid was carefully removed using a sterile syringe. Cells

in a sterile syringe were collected by filtering through a 0.22-micron filter membrane. The precipitates were collected by filtering through a 10-micron filter membrane and subjected to three gentle washes times with Milli-Q water prior to subsequent analysis.

The crystallographic structure of rhodochrosite was identified using a Powder X-ray Diffractometer (XRD, RigakuD Max-2550pc, Tokyo, Japan). Precipitates (about 0.5 g) were collected and washed several times until the supernatant was clarified, resulting in a white-yellowish precipitate. These precipitates were dried at 55 °C, ground to powder, and scanned in the 2θ ranging from 10° to 80°. The software utilized for analyzing the obtained spectra was MDI Jade 9.

The morphology and elemental composition were examined by scanning electron microscope (SEM, JSM-7500 F, Tokyo, Japan) and energy dispersive spectrometer (EDS, EMPYREAN, ICA, London, UK). The membrane samples contained precipitates, and cells were fixed by 2.0% glutaraldehyde overnight, followed by dehydration in increasing concentrations of ethanol. Subsequently, critical point drying was performed before applying a fine layer of gold coating for SEM-EDS analysis.

2.4. Heavy Metal Tolerance Ability, Motility and Biofilm Formation

The marine agar (MA) medium was employed to assess the tolerance ability of heavy metal, whereby varying concentrations of Cd^{2+} (0, 0.1, 0.5, 1, and 2 mM), Co^{2+} (0, 0.5, 1, and 2 mM), Cu^{2+} (0, 0.5, 1, and 2 mM), Hg^{2+} (0, 0.01, 0.05, 0.1, 0.5, 1, and 2 mM), Mn^{2+} (0, 10, 20, 50, 100, and 200 mM), or Zn^{2+} (0, 0.5, 1, 2, 10, and 20 mM) were incorporated as supplementary additions [21]. The presence of flagellum was examined using transmission electron microscopy (TEM, JEM-1230, JEOL, Tokyo, Japan). The motility was tested using the hanging drop method. To assess the biofilm formation of two strains, cells were collected after 3 days of cultivation in an MB medium supplemented with 20 mM Mn^{2+} without shaking. The biofilm was washed with phosphate buffer (pH 7.3), air-dried stained with crystal violet (0.1%) for 1 min, and washed with deionized water. Media without bacteria inoculation was used as a negative control.

2.5. Urea Hydrolytic Activity and EPS Production

Urea hydrolysis activity of strains Ery5 and Ery15 was detected in Christensen's Urea Agar with and without 2% urea. The medium contained (L^{-1}) casamino acid 1 g/L, sucrose 1 g/L, KH_2PO_4 2 g/L, NaCl 20 g/L, YE 0.01 g/L, phenol red 0.012 g/L, and agar 20 g/L. The pH was adjusted to 7.2. The medium was supplemented with filtered urea, achieving a final concentration of 2%. The change in color was an indication of the qualitative hydrolysis of urea. Media without urea was used as a negative control.

Qualitative EPS production was evaluated using a modified Congo red medium. Congo red medium was modified according to Freeman et al. [22] containing tryptone soya broth 37 g/L, sucrose 50 g/L, agar 10 g/L, and Congo red indicator 8 g/L. The Congo red solution was autoclaved separately. Strains were inoculated and cultured at 30 °C for 3 days. The presence of black colonies exhibiting a dry and crystalline consistency indicates positive EPS production [23].

2.6. Morphological, Physiological, and Chemotaxonomic Characteristics

The morphological characteristics of strains Ery5 and Ery15 were examined by cultivating on MA medium for a duration of 3 days. This examination involved the observation of various traits, including colonial size, shape, edge morphology, presence of bulges, level of transparency, and color properties. Cell morphology was examined by transmission electron microscopy (JEM-1230, JEOL, Tokyo, Japan). The anaerobic growth was conducted using an Anaerobic pouch (Mitsubishi Tokyo, Japan) on an MA medium supplemented with two electron acceptors, namely sodium nitrate and sodium nitrite. The Gram reaction, oxidase, and catalase activities, as well as hydrolysis of gelatin, starch, and Tween 20 and 40, were examined following the methodology described by Dong and Cai [24]. The growth temperature range was determined by incubating at various temperatures, including 4,

15, 20, 28, 30, 37, 45, and 50 °C. The pH tolerance for growth was evaluated in MB by adjusting the pH level within a wide spectrum from a minimum value of 5.0 to a maximum value reaching up to 10.5, with an increment interval of every 0.5 pH units using diverse buffer including MES (pH 5.0–6.0), PIPES (pH 6.5–7.0), Tricine (pH 7.5–8.5), or CAPSO (pH 9.0–10.5) at a concentration of 50 mM. The optimal conditions for growth in the presence of NaCl were determined by MB without NaCl but with varying concentrations of NaCl (ranging from 0 to 0.5, 1.0, 3.0, 5.0, 7.5, 10.0, and 15.0% as final concentration, *w/v*). The growth was evaluated using a UV/Visible Spectrophotometer (Ultrospec 6300 pro, Amersham Biosciences, Amersham, UK) by quantifying the optical density at 600 nm (OD_{6000}). The growth thresholds were determined based on the absence of any observable growth after a 30-day incubation period.

The identification of carotenoid-type pigments was conducted using the pigment absorption spectrum analysis method outlined by Hildebrand et al. [25]. Pigments were extracted with acetone/methanol (7:2, *v/v*) and performed using a Beckman DU 800 Spectrophotometer (absorption spectrum from 300 to 1000 nm). The BM medium was employed to assess the utilization of carbohydrates as the sole carbon and energy sources [26]. The medium was supplemented with complex nutrients (yeast extract, peptone, and tryptone, 0.2%, *w/v*), sugar (0.2%, *w/v*), alcohol (0.2%, *w/v*), organic acids (0.1%, *w/v*), or amino acids (0.1%, *w/v*) that was filter-sterilized. The acid production was assessed by employing the marine oxidation–fermentation (MOF) medium with an addition of 0.5% sugars [27]. API ZYM, API 20NE, and API 20E tests (bioMé rieux) were used to determine additional physiological and biochemical characteristics according to the manufacturer's instructions. The strips were exposed to a concentrated bacterial solution (MacFarland 5 standard) in an AUX medium supplemented with 2% (*w/v*) sea salts from Sigma (Burbank, CA, USA) [28]. API ZYM strips were read after 24 h, while API 20 NE and API 20 E strips were read after 48 h. The susceptibility to antimicrobial agents was evaluated using a two-tiered agar diffusion method [29]. Three reference strains, namely *C. marinus* E4A9[T], *C. mobilis* Ery22[T], and *C. pelagius* Ery9[T], were used as references in the above tests.

The FAME analysis cells were placed on MA from the quadrant and incubated at a temperature of 30 °C for a duration of three days. The analysis was conducted following the instructions of the Microbial Identification System. Isoprenoid quinones were extracted from freeze-dried cells (200 mg) using a chloroform and methanol mixture (2:1), followed by subsequent LC-MS (Agilent, Santa Clara, CA, USA) analysis [30]. Analysis of polar lipids was performed by DSMZ (Deutsche Sammlung von Mikroorganismen und Zellkulturen GmbH, Bonn, Germany). The total lipid material was quantified using molybdatophosphoric acid, while specific functional groups were identified via the application of spray reagents tailored to target defined functional groups [31,32].

2.7. Genome Sequencing and Analysis

High-quality genomic DNA was acquired using the AxyPrepTM Bacterial Genomic DNA Miniprep Kit (Axygen®, Corning, New York City, NT, USA), following the manufacturer's instructions. The 16S rRNA gene sequences were obtained by PCR with the universal primers 27F (5′-AGAGTTTGATCCTGGCTCAG-3′) and 1492R (5′-GGCTACCTTGTTA-CGACTT-3′). The SMRT technology with a PacBio RS II platform (Zhejiang Tianke Co., Ltd., Hangzhou, China) was utilized to sequence the genomes of both strains. The reads were de novo assembled using HGAP Assembly version 2 (Pacific Biosciences, Menlo Park, CA, USA). The verification process entailed confirming the circularization of the final contigs while simultaneously removing any overlapping termini to improve accuracy. The authenticity of the complete sequence of the 16S rRNA gene was confirmed by comparing it with PCR-derived gene sequences, following annotation using RNAmmer 1.2 Server [33].

The Rapid Annotation using Subsystem Technology (RAST) online server (https://rast.nmpdr.org/rast.cgi (accessed on 11 November 2022)) [34] was employed for the

annotation of the entire genome, obtaining information encompassing predicted coding sequences (CDSs), proteins, and RNAs. The KEGG database and KAAS webserver (https://www.genome.jp/tools/kaas/ (accessed on 6 March 2023)) were used for the functional annotation of genes and metabolic pathways [35].

The complete 16S rRNA sequence of strain Ery5 and Ery15 were identified in the EzBioCloud database [36]. Based on the obtained EzBioCloud results, the MEGA 11 software [37] package was employed for the construction of phylogenetic trees, incorporating 16 type strains from closely related species. Sequence data were aligned with CLUSTAL W. The MEGA 11 program package was employed to construct phylogenetic trees using the neighbor-joining (NJ), parsimony (MP), and maximum-likelihood (ML) methods. Evolutionary distances were calculated using the Kimura two-parameter model algorithm to implement the NJ method.

A phylogenomic tree of strains Ery5, Ery15, and its related taxa of the genus *Croceicoccus* was constructed based on single-copy orthologous clusters (OCs). The genome sequence needed was downloaded from the NCBI database. Proteins of all genome sequences were annotated by prokka [38]. OCs of all FAA documents were screened by Proteinortho (version 5.16b) [39]. The OCs obtained were modified and refined using MAFFT (version 7) [40] and trimAL (version 1.4.1) [41], respectively. According to the optimal replacement model prediction results, more than 800 models were predicted by IQ-Tree software (version 1.6.1) [42]. According to the predicted results, the ML phylogenetic tree was reconstructed using the LG+F+R5 model and visualized by applying MEGA 11 software.

The average nucleotide identity (ANI) between two genomes was calculated using the algorithm of the EZBioCloud web service [43]. The DNA–DNA hybridization (DDH) was estimated via genome-to-genome distance by GGDC [44]. Unique proteins harbored by the two strains were identified based on the results generated by OrthoMCL [45]. Classification of some predicted genes was analyzed using the COG database [46].

3. Result

3.1. Heavy Metal Resistance and Removal Ability of Mn^{2+}

Strains Ery5 and Ery15 were able to grow on MA solid plate medium with high concentrations of heavy metals, such as Mn (100.0 mM), Co (1.0–2.0 mM), Cu (1 mM), Zn (1.0 mM), Cd (0.5 mM), and Hg (0.1 mM) on MA.

The growth curves of the two strains at different concentrations of Mn^{2+} (Figure 1) indicated that the growth of strain Ery5 with a certain Mn^{2+} concentration range (10, 20, and 25 mM) was slightly better than that of without Mn^{2+}. The results showed that Mn^{2+} could promote the growth of bacteria at low Mn^{2+} concentrations, which was consistent with previous reports [18]. A significant growth inhibition occurred when the concentration was more than 30 mM for strain Ery5 and 33 mM for strain Ery15. In addition, no growth was observed when the Mn^{2+} concentration exceeded 50 mM for strain Ery5 and 35 mM for strain Ery15. The decrease in microbial activities may be attributed to the increased initial Mn^{2+} concentration, which ultimately led to heavy metal toxicity inhibiting bacteria growth.
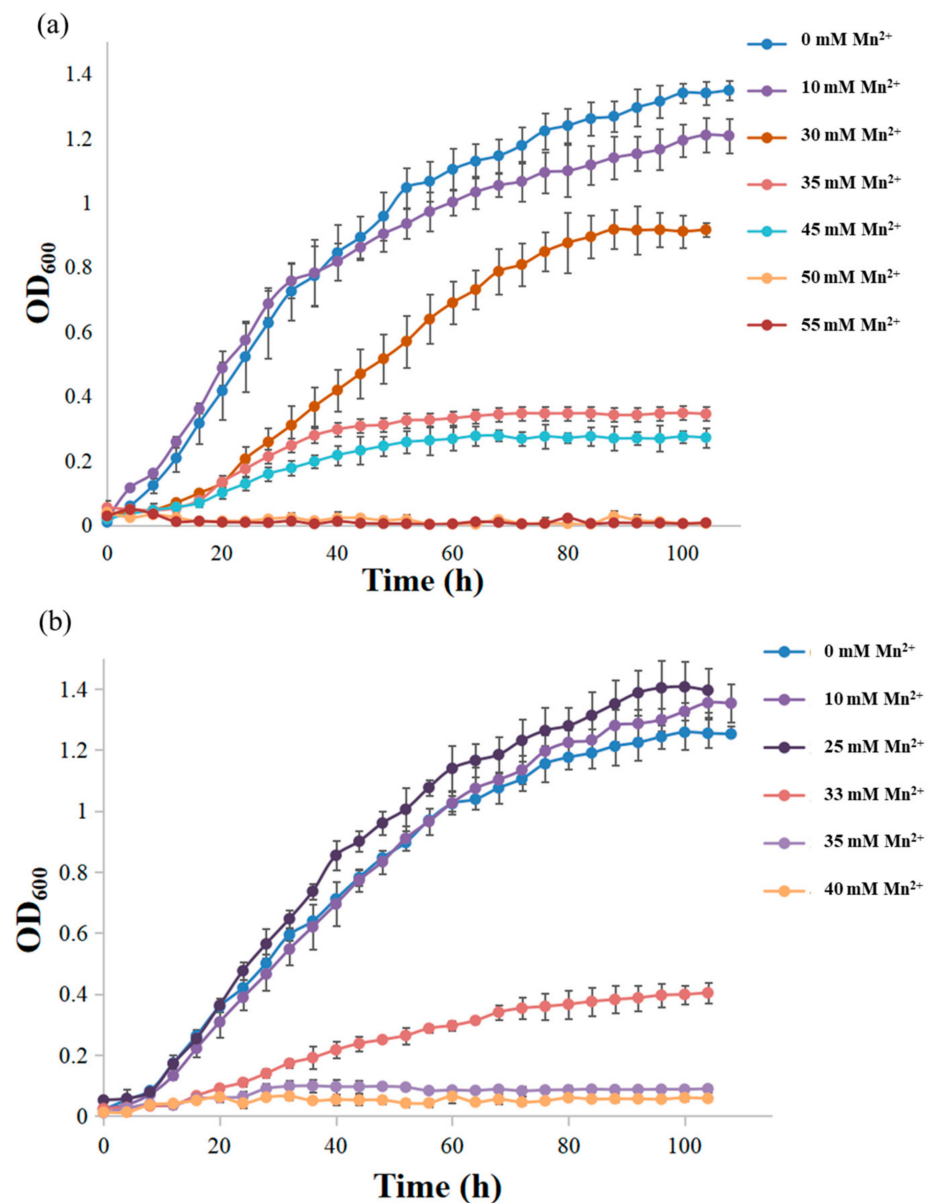
Figure 1. Effect of Mn^{2+} concentration on the growth of strains. (**a**) Ery5; (**b**) strain Ery15.

Based on the growth curve of Ery5 and Ery15 with and without urea (Figure 2), the growth of strain Ery5 in the presence of 2% urea was similar to the growth without the presence of urea at 10 and 30 mM of Mn^{2+}. However, when the concentration of Mn^{2+} exceeded 35 mM, the growth of strain Ery5 in the presence of 2% urea showed a significant improvement compared to the growth without the presence of urea. The growth was completely inhibited at 50 mM and 55 mM of Mn^{2+} in the absence of urea. However, when urea was present, noticeable growth was observed, with the OD_{600} reaching 0.7 and 0.5, respectively. Strain Ery15 also exhibited a similar growth pattern. The growth in the medium supplemented with urea was enhanced at 33, 35, and 40 mM Mn^{2+}.
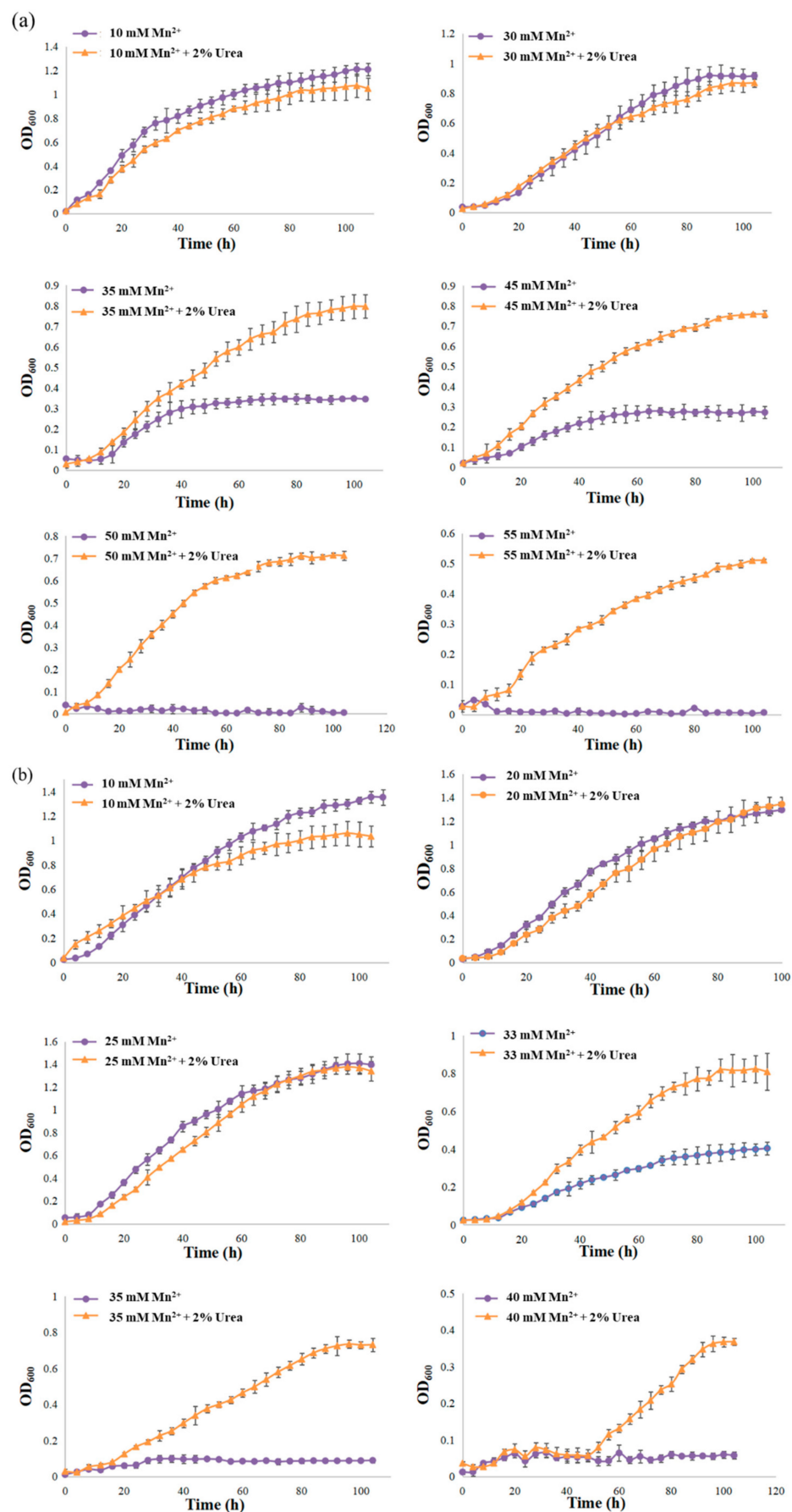
Figure 2. Effect of urea on the growth of strains. (**a**) Ery5; (**b**) Ery15.

These two strains were able to remove Mn^{2+} and decrease its concentration. The cell densities of strain Ery5 were similar (Figure 1) at 10 mM and 30 mM of Mn^{2+}, and the strain exhibited removal efficiencies of 31.34% and 26.16%, respectively. Similarly, the cell densities of strain Ery15 were similar (Figure 1) at 20 mM and 25 mM of Mn^{2+}, and the removal efficiencies of strain Ery15 were 28.74% and 28.59%, respectively. These observations could be attributed to the adsorption of cells or precipitation of rhodochrosite. The addition of urea could enhance the removal efficiency of Mn^{2+} (Figure S2). The growth of Ery5, with or without 2% urea, showed similar results on 10 mM or 30 mM Mn^{2+}, with the removal efficiency increasing from 31.34% to 41.44% and 26.16% to 30.72%, respectively. Similarly, the growth of Ery15, with or without 2% urea, showed similar results on 20 mM and 25 mM Mn^{2+}, with the removal efficiency increasing from 28.74 to 38.13% and 28.59% to 32.90%, respectively. These findings suggested that the presence of urea promotes the ability of strains Ery5 and Ery15 to remove Mn^{2+}.

3.2. Crystallographic Structure and Elemental Composition

The precipitates generated by strains Ery5 and Ery15 exhibited similar XRD patterns (Table S1, Figure S3). The diffraction peaks closely matched the rhodochrosite crystalline reference data (reference code 01-084-6983). The results suggested that particles obtained from strains Ery5 and Ery15 were rhodochrosite. The slight shifting of the diffraction peaks observed between the precipitate and reference data could potentially be attributed to the volume effect of the strains and the effect of MnCl2 concentration [47].

The morphology of precipitates characterized by scanning electron microscopy (SEM) revealed that ellipsoid-shaped crystals with multiple holes on the surface (Figure 3). The diameter of these holes was similar to the width of the cells, and fragments of cells were found within these holes (Figure 3). This observation is consistent with the previous reports that imprints matching the cell diameters were observed on the surface of $CaCO_3$ minerals [48]. In addition, no micrometer-sized carbonate crystals were observed on the cell surfaces. Previous studies have shown that cells involved in MICP are typically covered by sub-micrometer particles [20]. One possible explanation was that during the progress of precipitate formation, larger precipitates ranging from microns to tens of microns were formed, but accompanied by the disappearance of many relatively smaller precipitates (hundreds of nanometers) [49].

The elemental composition of the precipitates induced by strains Ery5 and Ery15 were found to be similar. The precipitates formed by strain Ery5 were primarily composed of C (21.30%), O (60.65%), Mn (17.37%) and Ca (0.61%). Similarly, the precipitates formed by strain Ery15 were composed of C (21.04%), O (60.52%), Mn (17.52%), and Ca (0.92%). The ratio of metal ions, C and O, was 1:1:3, indicating that the precipitates were mainly Mn- and Ca-containing carbonates.

The elemental composition of fragments in the holes or above the precipitates was collected by EDS (Figure 3). Biological elements, such as C, O, N, and S, were detected at these locations. The fragments formed by strain Ery5 were primarily composed of C (23.61%), N (3.92%), O (64.94%), Mn (7.33%), and S (0.19%). Similarly, the fragments formed by strain Ery15 mainly consisted of C (22.55%), N (2.52%), O (63.17%), Mn (11.45%), and S (0.31%). The proportion of C and O elements to metal ions was significantly higher than that of carbonate, suggesting that they may originate from residual cell tissues. Previous studies have shown that the composition of elements collected from the surface of mineral-coated cells has a high content of C and O elements, which aligned with the findings of this study [20]. EDS results indicated that the fragments in the holes or above the precipitated surface were cell fragments.
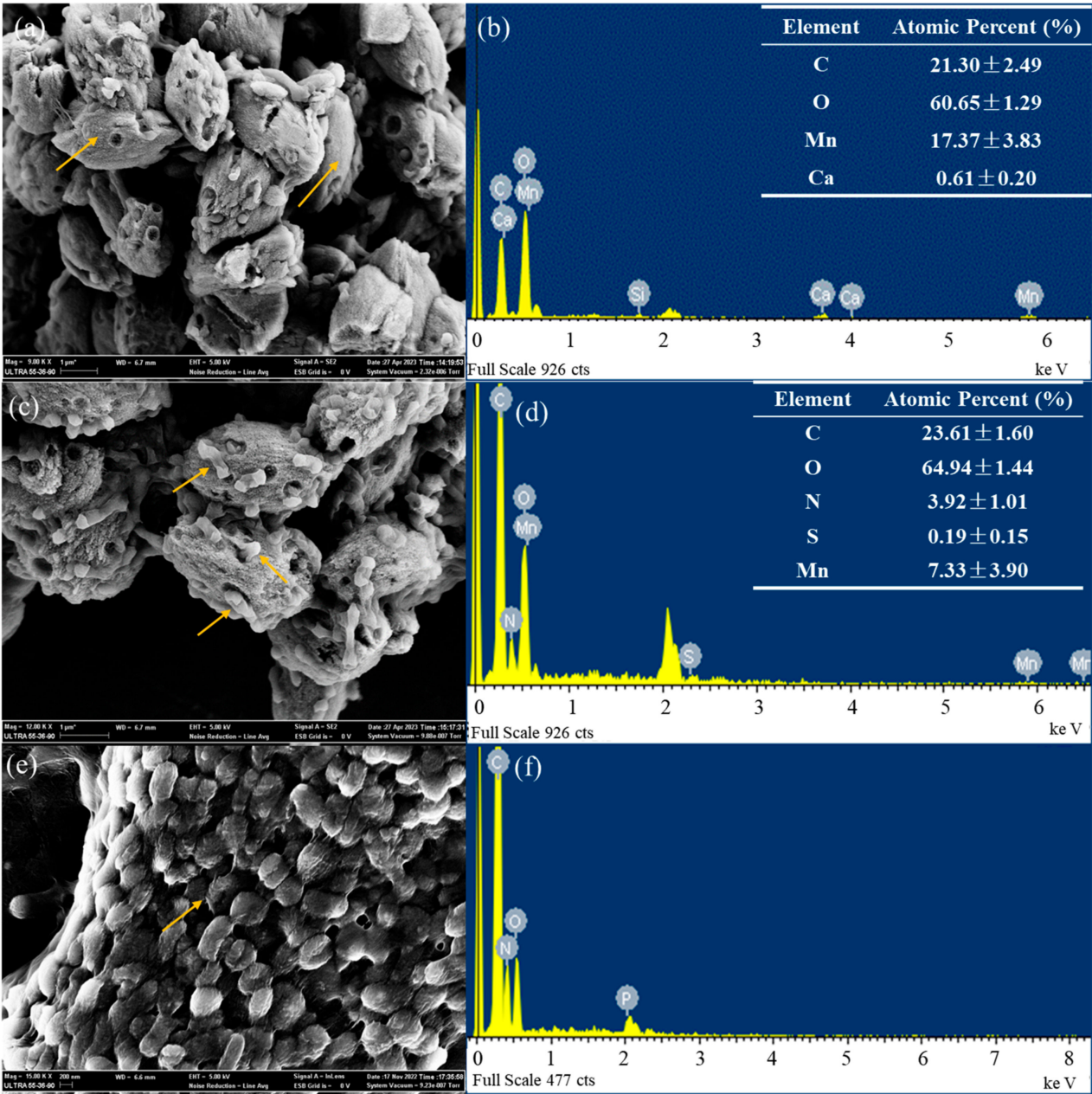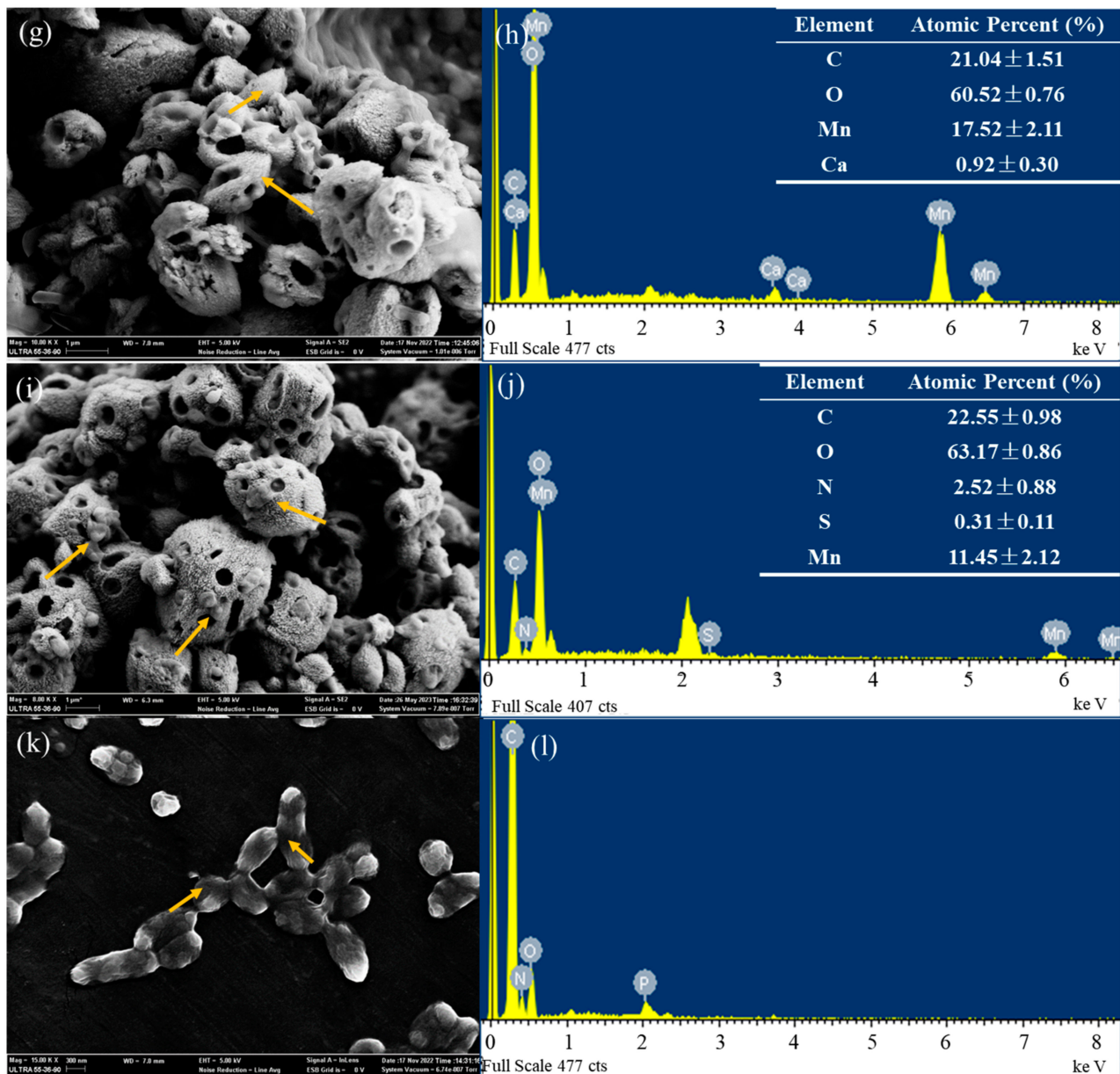
Figure 3. *Cont.*

Element	Atomic Percent (%)
C	21.04 ± 1.51
O	60.52 ± 0.76
Mn	17.52 ± 2.11
Ca	0.92 ± 0.30

Element	Atomic Percent (%)
C	22.55 ± 0.98
O	63.17 ± 0.86
N	2.52 ± 0.88
S	0.31 ± 0.11
Mn	11.45 ± 2.12

Figure 3. Morphology and elemental composition: (**a**,**c**) SEM images of precipitation produced by strain Ery5; (**b**,**d**) EDS analysis of arrow areas; (**e**) SEM images of cells of strain Ery5; (**f**) EDS analysis of cells of strain Ery5; (**g**,**i**) SEM images of precipitation produced by strain Ery15. (**h**,**j**) EDS analysis of arrow areas; (**k**) SEM images of cells of strain Ery15; (**l**) EDS analysis of cells of strain Ery15.

3.3. Morphological, Physiological, and Chemotaxonomic Characteristics

The SEM results showed that cells of strains Ery5 and Ery15 were rod-shaped, with a width ranging from 0.4 to 0.7 µm and a length ranging from 1.3 to 1.9 µm. Additionally, both strains exhibited motility via flagellum (Figure S4) and were capable of forming a biofilm. Furthermore, strains Ery5 and Ery15 were classified as EPS producers based on the Congo red test and possessed urea hydrolysis activity.

The species description provided below encompasses the physiological and biochemical aspects of both strains Ery5 and Ery15. The physiological and biochemical characteristics of the two strains and reference strains were presented in Table 1, facilitating a comparative analysis. For instance, the two isolates were Gram stain-negative, aerobic, rod-shaped, and did not contain Bchl *a*. Colonies of strain Ery5 appeared yellow after 3 days of incubation on MA, while colonies of strain Ery15 were cream colored. Both

strains, Ery5 and Ery15, showed optimal growth at temperatures ranging from 30 to 37 °C. Additionally, the optimum NaCl concentration for strains Ery5 and Ery15 were 5.0% and 1.0% (*w/v*), respectively.

Table 1. Differential phenotypic characteristics of strains Ery5, Ery15, and the type strains of their close relatives. Strains/species: 1, strain Ery5; 2, strain Ery15; 3, *C. marinus* E4A9[T]; 4, *C. pelagius* Ery9[T]; 5, *C. mobilis* Ery22[T]; All data were acquired from this study unless otherwise specified. +, Positive; −, negative; w, weak.

Characteristics	1	2	3	4	5
Color	Yellow	Cream	Yellow	Yellow	Yellow
Nitrate reduction	−	−	−	+	−
H_2S production	+	−	+	−	−
Urea hydrolysis	+	+	−	−	+
Tryptophane deaminase	+	+	+	w	+
Utilization of					
L-Arabinose	+	−	+	−	−
Capric acid	+	+	+	+	+
Glucose	−	w	+	+	+
Maltose	−	−	+	+	+
Malate	−	−	−	−	+
Mannitol	−	−	−	+	+
Acid production:					
Ethanol	−	+	−	−	−
D-Galactose	−	−	+	−	−
D-Xylose	−	−	+	−	−
Enzyme activities:					
α-Chymotrypsin	−	−	−	−	+
Cystine arylamidase	+	−	+	w	+
Esterase (C4)	+	+	+	+	−
Esterase lipase (C8)	+	+	+	−	+
α-Galactosidase	−	−	+	−	−
β-Galactosidase	−	−	+	−	−
α-Glucosidase	−	−	+	+	+
β-Glucosidase	−	−	+	−	−
β-Glucuronidase	+	−	+	−	−
Trypsin	−	−	−	−	+
Valine arylamidase	+	+	+	+	+
Antibiotic susceptibility:					
Ampicillin (10 µg)	w	−	+	+	−
Erythromycin (10 µg)	+	+	+	+	+
Neomycin (30 µg)	+	−	+	w	+
Nitrofurantoin (300 µg)	+	−	+	+	+
Penicillin (10 IU)	−	−	+	+	−
Tetracyline (30 µg)	−	−	+	w	w
DNA G+C content (%)	62.5	62.2	64.0	62.8	62.5

The major respiratory quinone found in both strains was ubiquinone-10 (Q10), consistent with other members of the genus *Croceicoccus* [13,14]. Analysis of fatty acids revealed that two strains contained a high value of $C_{18:1}\omega7c$ (56.6% and 49.4%), similar to the *C. marinus* E4A9[T], *C. pelagius* Ery9[T], and *C. mobilis* Ery22[T] (24.4–45.8%). In addition, two isolates and the reference strains possessed $C_{14:0}$ 2OH (13.3% and 15.7%) as the major fatty acids (Table 2).

Table 2. Fatty acid composition (%) of strains Ery5, Ery15, and the type strains of their close relatives. Strains/species: 1, strain Ery5; 2, strain Ery15; 3, *C. marinus* E4A9[T]; 4, *C. mobilis* Ery22[T]; 5, *C. pelagius* Ery9[T]. All data were taken from this study. -, Not detected; tr, traces ($\leq$0.5%).

Fatty Acid (%)	1	2	3	4	5
Straight-chain					
$C_{14:0}$	1.3	1.6	2.1	1.4	1.4
$C_{15:0}$	tr	tr	2.1	1.0	tr
$C_{16:0}$	4.5	4.3	2.7	11.8	2.1
Unsaturated					
$C_{15:1}\omega6c$	-	-	0.9	-	-
$C_{16:1}\omega5c$	1.5	1.1	0.7	0.9	2.0
$C_{17:1}\omega8c$	0.8	1.2	1.8	-	-
$C_{17:1}\omega6c$	4.6	6.3	16.9	6.1	1.9
$C_{18:1}\omega7c$	56.6	49.4	26.0	45.8	24.4
$C_{18:1}\omega5c$	2.0	2.3	3.3	1.5	1.7
11 methyl $C_{18:1}\omega7c$	1.8	1.8	-	0.7	0.6
Hydroxy					
$C_{13:0}$ 2OH	-	-	0.6	-	-
$C_{14:0}$ 2OH	13.3	15.7	22.2	16.9	41.9
$C_{15:0}$ 2OH	1.6	2.2	5.5	2.1	2.7
$C_{16:1}$ 2OH	-	-	-	-	1.6
iso-$C_{16:0}$ 3OH	1.2	0.6	-	0.5	2.5
$C_{16:0}$ 2OH	2.5	1.6	-	-	5.8
$C_{18:1}$ 2OH	0.8	tr	-	-	1.4
Cyclic					
$C_{19:0}\omega8c$ cyclo	tr	1.9	4.6	-	-
Summed Feature *					
3	7.0	9.4	10.7	11.1	9.0

* Summed feature 3 contained $C_{16:1}\omega7c$ and/or iso-$C_{15:0}$ 2OH that could not be separated by GLC with the MIDI system.

The major polar lipids of strain Ery5 are phosphatidylcholine, two sphingoglycolipids, one unidentified phospholipid, and one unidentified glycolipid. The major polar lipids of strain Ery15 are two sphingoglycolipids, one unidentified phospholipid, and one unidentified glycolipid. Compared with the reference strains, they both possessed two sphingoglycolipids as the major compounds. In addition, two isolates and the reference strains possessed phosphatidylcholine, phosphatidylethanolamine, phosphatidylglycerol, and one unidentified phospholipid. However, one unidentified glycolipid (GL1) as the major lipid for the two isolates was absent for *C. marinus* E4A9[T] (ref. [14] and Figure S5).

3.4. General Genome Characteristics and Phylogenetic Properties

The combined genome sizes of the Ery5 and Ery15 strains were 3.84 Mb and 3.63 Mb, respectively. The G+C content of the DNA extracted from strain Ery5 was determined to be 62%, falling within the reported range for *Croceicoccus* genus members, i.e., 62.5–64.5% [50]. The DNA G+C content of strain Ery15 was 62.2%, which is slightly lower than the range reported. The general genomic features of strains Ery5 and Ery15 are shown in Table S2.

The complete 16S rRNA gene sequence of strains Ery5 and Ery15 (1446 nt) was obtained from the genome sequence. The 16S rRNA sequences of strains Ery5 and Ery15 exhibited a similarity ranging from 98.1% to 95.7% with those of other strains in the genus *Croceicoccus*, revealing that the two strains may represent a novel species in this genus (Table S3). The phylogenetic trees, reconstructed with the NJ, ML, and MP methods based on the genetic sequences of the 16S rRNA gene, indicated that strains Ery5 and Ery15 fall into the clade that consists of *Croceicoccus* species. They form a distinct cluster alongside *C. marinus* E4A9[T] and *C. mobilis* Ery22[T] (Figure 4), representing an autonomous lineage. In addition, the strains Ery5 and Ery15 exhibited a 100% similarity in their 16S rRNA gene sequences, forming a robust lineage with a high bootstrap (100%). The rRNA gene sequences underwent BLAST analysis, revealing complete sequence identity between the

5S and 16S rRNA genes of both strains. Furthermore, a high similarity score of 99.3% was observed for the 23S rRNA gene sequences between the two strains.
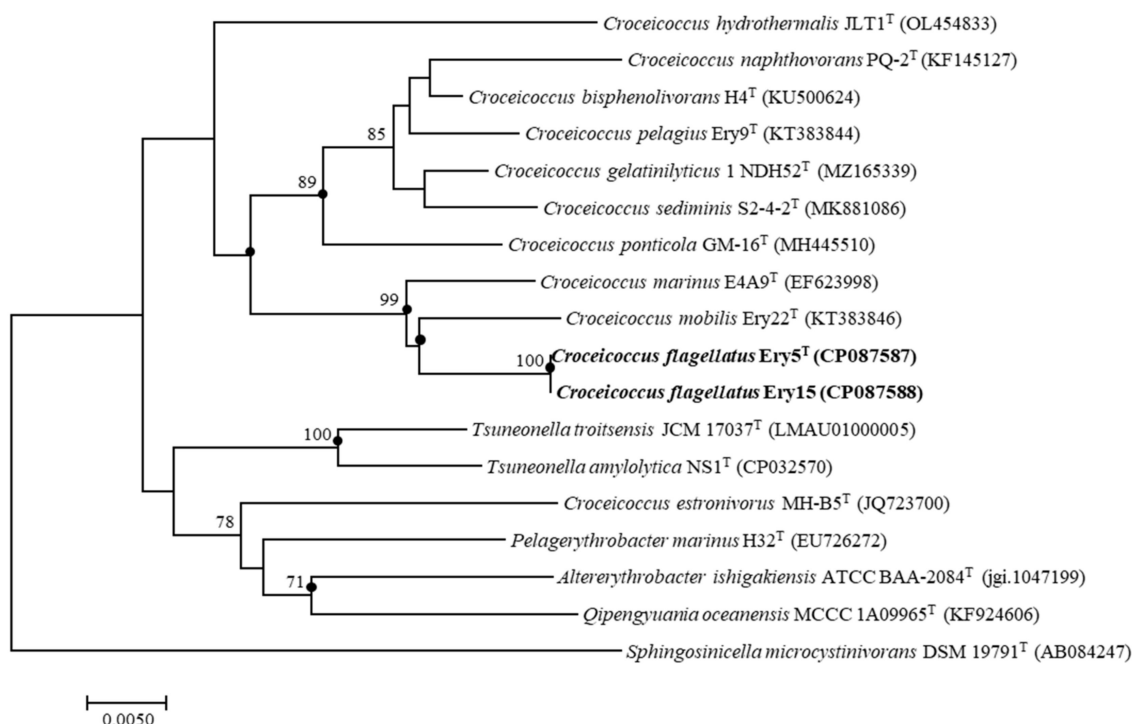
Figure 4. The NJ phylogenetic tree was constructed using 16S rRNA gene sequences to depict the taxonomic relationships between the isolate and other closely related taxa. The branch nodes are accompanied by bootstrap values (>70%) based on 1000 replications. Circles denote consistent identification of these nodes in trees generated via ML and MP algorithms. Bar, 0.005 substitutions per nucleotide position.

Genomes of the type strains belong to the genus *Croceicoccus*, and five other genomes from the family *Erythrobacteraceae* were selected for phylogenomic tree analysis. The phylogenomic tree based on concatenated 844 protein sequences from genomic sequences showed similar topologies with phylogenetic trees (Figure S6).

The ANI values and the genome-to-genome distance between strain Ery5 and reference strains are 75.2–82.9% and 20.6–25.9%, respectively (Table S4). The ANI values and the genome-to-genome distance between strain Ery15 and reference strains are 77.0–83.0% and 21.3–25.6%, respectively (Table S4). These ANI values were far below the threshold of species boundary (95–96%) [51], and genome-to-genome distance values were well below the 70% cut-off [52], indicating a low taxonomic relatedness between strains Ery5 and Ery15 and reference species. The ANI values and genome-to-genome distance between strain Ery5 and strain Ery15 were 95.5% and 63.8%, respectively, which were close to the threshold of the species boundary (95–96% for ANI values and 70% for in silico DDH) [53,54]. In addition, the OrthoMCL results showed that 20% of unique proteins were found in the genomes of strains Ery5 and Ery15 (Figure S7). Numbers and ratios of category L detected in strain Ery15 were threefold higher than strain Ery5. Category L represents genes involved in replication, recombination, and repair, which make it easier for the strain to acquire foreign genes and react against external changes in the novel habitats. Strain Ery15 might acquire more foreign genes to adapt to the environment.

3.5. Genes Related to Motility, Chemotaxis, and Biofilm Formation

The SEM results demonstrated that strains Ery5 and Ery15 exhibited motility via flagellum (Figure S4). The genomes of strains Ery5 and Ery15 comprised 35 genes associated with flagellar assembly, including the complete set of genes for flagellar biosynthesis and

flagellar structure proteins. The genome harbored regulatory elements governing flagellar synthesis (Flgm, FlrC, and Flia). In addition, genes encoding chemotaxis proteins involved in motility, such as CheAWRBYZ and methyl-accepting chemotaxis protein, were present.

The results of crystal violet staining indicated that strains Ery5 and Ery15 were capable of forming biofilm. The genomes of the two strains contained numerous genes that were involved in the process of biofilm formation. It was well established that flagella, EPS, and other outer membrane adhesins play a crucial role in the development of biofilms [53–55]. Previous studies have demonstrated the significance of *flrC*, which can influence bacterial adhesion via motility and chemotaxis [56]. During the process of biofilm development, the synthesis of colanic acid was necessary for the formation of EPS. It has been observed that the synthesis of colanic acid played crucial role in the surface expression and assembly of EPS [57–61]. The *wza* genes responsible for the synthesis of colanic acid were annotated in the genomes of strains Ery5 and Ery15. The role of quinolone signal (QS) in controlling biofilm formation via the regulation of EPS synthesis has been demonstrated. The key genes *trpE* (K01657) and *trpG* (K01658), involved in the production of a typical QS [62], were detected in the genomes of strains Ery5 and Ery15. In addition, regulators related to biofilm formation were annotated in the genome of strains Ery5 and Ery15. The gene *csgD* acted as a master regulator of biofilm formation in certain species [63]. Another gene, *rpoN*, also contributes to the formation of biofilm by its regulation of the synthesis of a biofilm-stabilizing EPS [64].

Moreover, in the genomes of strain Ery5 and Ery15, 13 and 9 CDSs encode GGDEF (diguanylate cyclase), EAL (diguanylate phosphodiesterase), and PAS (Per-Arnt-Sim) domains, respectively. These domains have been demonstrated to have significant involvement in biofilm formation and motility processes.

3.6. Genes Related to REDOX and Metal Transporters

Manganese, copper, cobalt, and zinc are essential elements, but they can become toxic when present in excessive amounts. Mercury, lead, and cadmium were considered toxic even at low concentrations [65]. Strains Ery5 and Ery15 exhibited a high manganese resistance ability to heavy metal. The genomes of Ery5 and Ery15 strains were found to harbor a diverse array of genes associated with the transport of metal ions and redox processes (Table S5). Two major ways to cope with high concentrations of metal ions were detected by the strains Ery5 and Ery15 based on genomic data analysis.

One was the enzymatic detoxification process based on the use of either reducing or oxidizing metals, respectively, and plays a crucial role in the metal biogeochemical cycles. Several genes were identified in the genomes of strains Ery5 and Ery15. CopG protein was believed to have a role in interconverting Cu(I) and Cu(II), aiming to reduce potential toxicity and promote their removal via the efflux system [66]. Microorganisms employ multi-copper oxidases (MCOs) as regulatory mechanisms to mitigate the detrimental effects of metal ions by modulating their oxidation states in aerobic environments [67]. Seven and six MCOs were annotated in the genomes of strains Ery5 and Ery15 (Table S5). Specific MCO genes, such as *mopA*, *cueO*, *mcoA*, *moxa*, and *mmxG,* involved in Mn (II) or Mn (III) oxidation [68,69], were not annotated in the genome of strains Ery5 and Ery15.

Furthermore, microorganisms utilized metal transporters to maintain the balance of metal ion concentrations within cells. Dozens of genes potentially involved in transport efflux pumps and transcriptional regulators were identified in the genomes of strains Ery5 and Ery15. The concentration of the metal ions was maintained by the efflux system, including the RND efflux system, the cation transporters, and P-type ATPase. Firstly, the RND efflux systems mediated a highly efficient detoxification process. The Cus RND transporter (CzcCBA) was responsible for exporting Zn^{2+}, Co^{2+}, and Cd^{2+} cations from both the cytoplasm and the periplasm to the outside [70]. The operons of czcCBA were encoded by Strain Ery5, comprising a pair of czcC outer membrane protein genes, eight czcA inner membrane protein genes, and eight czcB membrane fusion protein genes. Additionally, strain Ery15 possessed an extra copy of *czcA* and *czcB*. The Cus RND transporter (CusCBA)

was responsible for exporting copper/silver ions [65]. Strains Ery5 and Ery15 possessed one and two operons of *cusCBA*, respectively. Secondly, the cation transporters located in the cytoplasm membrane may participate in transporting ions against their concentration gradient to the periplasm. Six and nine *czcD* genes, which may be potentially involved in the transport of cobalt, zinc, and cadmium, were annotated in the genomes of strains Ery5 and Ery15, respectively. Additionally, the genomes of strains Ery5 and Ery15 were found to have two and four *corC* genes, respectively, which may play a role in the transport of magnesium and cobalt. Thirdly, P-type ATPase is a single-subunit system located in the cytoplasmic membrane that uses energy to pump ions out of the cytoplasm. The genomes of strains Ery5 and Ery15 possessed five and six heavy metal transporting ATPase genes, respectively, which may be involved in the transport of lead, cadmium, zinc, and mercury ions across the cytoplasmic membrane. Furthermore, the MerR family of transcriptional regulators plays a pivotal role in modulating the activity of ATPases in response to intracellular heavy metal concentrations [66]. Three transcriptional regulator genes (*merR*) were annotated in the genomes of strains Ery5 and Ery15, which regulate detoxification processes.

These export systems in bacteria were capable of acting on a range of cations, such as Zn^{2+}, Co^{2+}, Cd^{2+}, Mn^{2+}, Cu^+, Cu^{2+}, Ag^{2+}, Hg^{2+}, and Pb^{2+}. These systems may be associated with the mechanism of heavy metal resistance. It has been suggested that strains Ery5 and Ery15 employed two main strategies to avoid the toxicity of heavy metals: converting the metal valence to a less toxic valence state [71] and pumping the ions out of cells [72].

3.7. Genes Related to Urea Hydrolysis Activity and Exopolysaccharide Production

The genomes of strains Ery5 and Ery15 lack urease (*ureABC*); however, they harbored genes responsible for urea decomposition, including encoding urea carboxylase and allophanate hydrolase. Additionally, the genomes of strains Ery5 and Ery15 contain urea carboxylase-related aminomethyltransferase and urea carboxylase-related ABC transporter, suggesting their capability of utilizing urea as a C or N source in the environment.

Furthermore, strains Ery5 and Ery15 are classified as EPS producers based on the Congo red test. EPSs are complex polysaccharides characterized by elongated chains comprising predominantly glucose, galactose, and rhamnose in varying proportions. A large array of genes associated with exopolysaccharide biosynthesis were annotated in the genomes of strains Ery5 and Ery15. Succinoglycan is a type of anionic exopolysaccharide. Strains Ery5 and Ery15 possess *exoA*, *exoP*, *exoZ,* and *exoV* genes, which are relevant to the biosynthesis of succinoglycan. Sphingan is a group of heteropolysaccharides that differ only in side chain, backbone monosaccharides, and decorations. Strains Ery5 and Ery15 possess genes related to the biosynthesis of Sphingan, including *dpsC*, *dpsD*, *welF*, *welG*, *welI,* and *rmlABCD*. Additionally, strain Ery15 has an extra *welB* gene. It can be inferred that strains Ery5 and Ery15 have the ability to synthesize diverse EPSs and distribute them on cell surfaces.

4. Discussion

4.1. Strategies to Adapt to Deep-Sea Environments with High Metal Concentrations

Heavy metal exposure can adversely affect prokaryotic cells by disrupting the structure and function of molecules, such as proteins and DNAs essential for biological processes [73]. Previous studies have highlighted the existence of manganese-tolerant bacteria, particularly those found in terrestrial metal mines [74,75]. With the discovery of deep-sea mineral resources and the increasing interest in deep-sea mining, there has been a rising concern regarding metal-resistant bacteria inhabiting the deep-sea environment. Scientists were particularly interested in understanding the mechanisms that allow these bacteria to tolerate and adapt to the deep-sea environment. In a study evaluating the diversity of heavy-metal resistant bacteria in both the deep-sea polymetallic nodule area and hydrothermal poly-metallic sulfide area, strains Ery5 and Ery15 with the ability to resist heavy metals and form rhodochrosite precipitates were screened as pure cultures for further study. To date, there have been a few reports of manganese-resistant bacteria found in deep-sea environments

(depth $\geq$ 1000 m). Among these, strains Ery5 and Ery15 exhibited the highest level of manganese resistance [76–81]. In addition, no microbial-induced rhodochrosite precipitation formation has been reported in deep-sea environments until now. Therefore, these two strains, which possess both heavy metal resistance and biomineralization capabilities, have great potential as candidates for bioremediation. Research on strategies to adapt to the deep-sea heavy metal environment will provide valuable insights for the treatment and restoration of the deep-sea mining environment.

The results of SEM and crystal violet staining confirmed that strains Ery5 and Ery15 exhibited resistance to heavy metals, the presence of flagellum, and biofilm formation. Genomic analysis further revealed that the genomes of both strains contained numerous genes and pathways associated with these processes. Therefore, it can be inferred that strains Ery5 and Ery15 employed various effective survival strategies to adapt to deep-sea environments with high metal concentrations. These strategies included motility, chemotaxis, biofilm formation, metal REDOX reactions, and transporters. The presence of flagella and the capacity for chemotaxis would confer significant advantages to strains as they navigate away from substances that exert detrimental effects on vital metabolic [82]. Biofilm can create a local microenvironment for cells embedded in biofilms [83]. The enzymatic detoxification process by reducing or oxidizing metals can help minimize the toxic effects and aid in their removal via the efflux system [65,84]. Metal transporters were used to transport metals from cells to maintain the balance of metal ion concentrations [85,86].

4.2. Mechanism of Rhodochrosite Precipitation Formation

Deep-sea mining may cause leaching of heavy metal ions into surrounding seawater, resulting in significant environmental impacts. To mitigate these effects, immobilizing metal ions in the deep-sea environment was considered an effective restoration approach. Microbial-induced rhodochrosite precipitation plays a critical role in the immobilization of Mn^{2+} in deep-sea environments. The analysis of the crystallographic structure and elemental composition of the participants revealed that strains Ery5 and Ery15 exhibited great potential in rhodochrosite precipitation. It can be inferred that strains Ery5 and Ery15 can secrete metabolites via their physiological activities to react with ions or compounds in the environment, such as EPS, biofilms, and some biomorphs can act as sites for ion adsorption and mineral deposition, thereby inducing mineralization processes [87].

Based on the ability of urea hydrolysis and EPS production of strains Ery5 and Ery15, it can be inferred that bacterial cells can promote the crystallization of carbonate by creating a supersaturated alkaline environment and secreting EPS. Microbial-induced rhodochrosite precipitation could be considered a special MICP and only reported by *Sporosarcina pasteurii* for the removal of heavy metal from water [12]. Strains Ery5 and Ery15 possessed the capability to decompose urea into ammonia and carbonates. During incubation, ammonia converted into NH_4^+ and released OH^-, thereby resulting in the alkalization of the media environment, which was essential for the biomineralization process (Figure 5). Previous studies have indicated that EPS directly influences the mineralogy of precipitation [49,88]. EPS was composed of carboxyl, amino, phosphate, and hydroxyl polysaccharides and proteins [89], which contain negatively charged functional groups that can bind Mn^{2+} ions [90]. These EPS molecules were distributed on cell surfaces and acted as effective heterogeneous nucleation sites, facilitating the binding of cations and initiating carbonate precipitation. Consequently, bacteria cells will serve as the core for crystal nucleation and growth [48,91]. This was followed by the generation of carbonate precipitation on the cell's surface [10,92,93]. According to the dominant theory of nucleation in the MICP process, bacteria utilized their own cells or cell walls as the nucleating centers during growth, resulting in the gradual formation of precipitates. When cells die and disintegrate, they create holes in the precipitation (Figure 3).
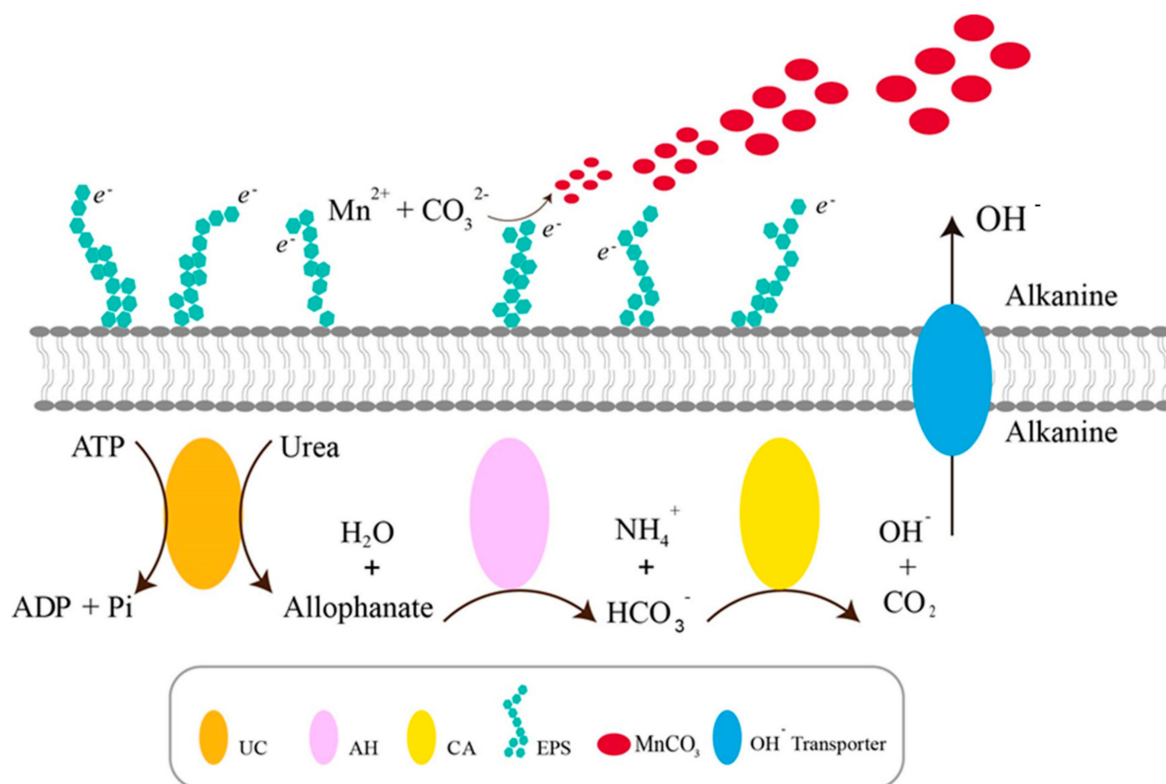
Figure 5. The mechanism of microbial-induced rhodochrosite precipitation.

4.3. Proposal of Novel Species

Strains Ery5 and Ery15 have high 16S rRNA gene sequence similarities (100%) (Table S3). Meanwhile, the two strains show a high similarity in fatty acid compositions. However, strains Ery5 and Ery15 could also be distinguished from each other. Firstly, the ANI value between strains Ery5 and Ery15 was on the threshold of the species boundary (95–96%), and the genome-to-genome distance was slightly below the species boundary (70%). There are 20% of unique proteins found in the genomes of strains Ery5 and Ery15. Secondly, strain Ery15 could be different from Ery5 by phenotypic characteristics differences, such as H_2S production, utilization of L-arabinose and glucose, acid production from ethanol, presence of cystine arylamidase and β-glucuronidase. The colonies were yellow for strain Ery5 and cream for strain Ery15. Thirdly, the polar lipid profiles also show some differences between strain Ery5 and strain Ery15[T] (Figure S5). Strain Ery5 contains one unidentified aminolipid and two unidentified glycolipids, which were not detected in strain Ery15. On the basis of phenotypic characteristics, genomic data, as well as chemotaxonomic data obtained in this study, indicated that these two strains were distinct strains rather than separate colonies.

Strains Ery5 and Ery15 could also be differentiated from the related species by phenotypic characteristics differences such as color, NaCl optimum, temperature range, nitrate reduction, H_2S production, urea hydrolysis, carbohydrates utilization, acid production, enzyme activities, and antibiotic susceptibility (Table 1). In this study, strains Ery5 and Ery15 represent a novel species within the genus *Croceicoccus*, for which the name *Croceicoccus flagellatus* sp. nov. is proposed.

Description of *Croceicoccus flagellatus* sp. nov.

Croceicoccus flagellatus (fla.gel.la'tus. L. masc. part. adj. *flagellatus*, flagellated).

Cells are Gram stain-negative, aerobic, and rod-shaped, 0.4–0.7 μm in width, and 1.3–1.9 μm in length. Flagella are observed. Colonies are yellow, circular, convex, smooth, and 1–2 mm in diameter after 3 days of incubation at 30 °C on MA. The color of strain Ery5[T] is yellow, while strain Ery15 is cream. Growth occurs on NaCl-free MB supplemented with 0–7.5% (*w/v*) NaCl (optimum 1.0–5.0%). The pH and temperature ranges for growth are pH

5.5–8.5 and 15–45 °C (optimum at pH 7.0 and 30–37 °C). Contain carotenoid-like pigments. Bchl *a* is absent. No anaerobic growth occurs on MA supplemented with potassium nitrate and sodium nitrite. Positive for catalase, oxidase, arginine dihydrolase, citrate utilization, tryptophan deaminase, urea hydrolysis, and Voges-Proskauer reaction. Negative for lysine and ornithine decarboxylases, indole formation, and nitrate reduction. Strain Ery5^T is positive for H$_2$S production, while strain Ery15 is not. Esculin, gelatin, and starch are not hydrolyzed. Acid and alkaline phosphatases, esterase (C4), esterase lipase (C8), leucine arylamidase, naphthol-AS-BI-phosphohydrolase, and valine arylamidase activities are present; *N*-acetyl-*β*-glucosaminidase, *α*-chymotrypsin, *α*- and *β*-galactosidases, *α*- and *β*-glucosidases, *β*-fucosidase, lipase (C14), and *α*-mannosidase, trypsin activities are absent. The presence of cystine arylamidase and *β*-glucuronidase varied. The following compounds are utilized as sole carbon and energy sources: capric acid, peptone, yeast extract, and tryptone. The utilization of L-arabinose and glucose varied. Acid is not produced from cellobiose, ethanol, D-fructose, D-galactose, glucose, *myo*-inositol, *α*-D-lactose, maltose, mannitol, D-mannose, D-melezitose, D-ribose, ribitol, L-rhamnose, raffinose, sorbitol, sorbose, sucrose, trehalose, and D-xylose. The production of acid from ethanol was observed in strain Ery15. The principal fatty acids (>5%) are C$_{18:1}\omega7c$, C$_{14:0}$ 2OH, and summed feature 3 (C$_{16:1}\omega7c$ and/or iso-C$_{15:0}$ 2OH). The sole respiratory quinone is ubiquinone 10 (Q-10). The major polar lipids are two sphingoglycolipids, one unidentified phospholipid, and one unidentified glycolipid. In addition, moderate to minor amounts of phosphatidylethanolamine, phosphatidylcholine, phosphatidylglycerol, one unidentified phospholipid, three unidentified glycolipids, and one unidentified lipid were also present. One unidentified aminolipid and two unidentified glycolipids were also detected in strain Ery15. The DNA G+C content is 62.2–62.5% (by the genome).

The type strain, Ery5^T (=CGMCC 1.15357^T = DSM 101477^T), was isolated from sediment collected from the polymetallic nodule region of the East Pacific Ocean at a depth of 5377 m. An additional strain, Ery15^T (=CGMCC 1.15359 = DSM 101480), was isolated from deep-sea sediment collected from the South Atlantic Rise at a depth of 2687 m. The GenBank accession numbers for the 16S rRNA gene and genome sequences of strain Ery5^T are KT383843 and CP087587, respectively. The GenBank accession numbers for the 16S rRNA gene and genome sequences of strain Ery15 are KT383845 and CP087588, respectively.

5. Conclusions

Strains Ery5 and Ery15 were obtained from deep-sea polymetallic nodule area and hydrothermal polymetallic sulfide area, respectively. Two strains exhibited high manganese resistant ability and rhodochrosite precipitation formation ability. Genomic analysis indicated that strains used several favorable survival strategies to cope with heavy metal environments, such as motility, chemotaxis, biofilm formation, metal redox, transporters, and so on. Based on the ability of urea hydrolysis and EPS production of strains Ery5 and Ery15, it is presumed that bacterial cells can promote crystallization of carbonate by creating a supersaturated alkaline environment and secreting EPS. In addition, strains Ery5 and Ery15 were identified by polyphasic taxonomy methods and proposed as a new species belonging to the genus *Croceicoccus*. This work provided potential candidates for bioremediation in deep-sea environments. The process of environmental restoration in deep-sea mining is highly intricate, necessitating the integration of deep-sea engineering technology and deep-sea environmental management. Further research in this field is crucial to advance the implementation of restoration projects.

Supplementary Materials: The following supporting information can be downloaded at: https://www.mdpi.com/article/10.3390/jmse11112195/s1, Figure S1: Locations of the two sampling sites of strains Ery5 and Ery15; Figure S2: Removal efficiency of Mn^{2+} in strains Ery5 and Ery15; Figure S3: XRD images of strains Ery5 and Ery15; Figure S4: Transmission electron micrographs of strains Ery5 and Ery15; Figure S5: Thin-layer chromatograms after staining with molybdatophosphoric acid showing the total polar lipid profiles of two strains; Figure S6: Maximum-likelihood tree based on concatenated 844 protein sequences from genomic sequences showing the phylogenetic relationship of the strains Ery5 and Ery15 with the related taxa; Figure S7: Comparison of COG profile of unique proteins; Table S1: Diffraction peaks location of XRD of strain Ery5 and Ery15; Table S2: Genomic features of Ery5 and Ery15; Table S3: The 16S rRNA gene sequence similarities between strains Ery5, Ery15 and the type strains of the genus *Croceicoccus*; Table S4: The ANI values and the genome-to-genome distance of strains Ery5, Ery15 and the type strains of their closely relatives; Table S5: Annotated genes with putative function in resistance to heavy metals between strains Ery5 and Ery15.

Abbreviations

ANI, average nucleotide index; CCZ, Clarion-Clipperton Zone; CDSs, coding sequences; DDH, DNA-DNA hybridization; EAL, diguanylate phosphodiesterase; EDS, energy dispersive spectrometer; EPS, extracellular polymeric substance; FAME, fatty acid methyl ester; ICP-OES, Inductively Coupled Plasma Optical Emission Spectrometer; ISA, International Seabed Authority; MA, marine agar; MB, marine broth; MCOs, multi-copper oxidases; MICP, microbial-induced carbonate precipitation; ML, maximum-likelihood; MOF, marine oxidation-fermentation; MP, maximum-parsimony; NJ, neighbor-joining; OCs, orthologous clusters; SEM, scanning electron microscope; PAS, Per-Arnt-Sim; XRD, Powder X-ray Diffractometer; TEM, transmission electron microscopy.

References

1. Hein, J.R.; Koschinsky, A.; Kuhn, T. Deep-ocean polymetallic nodules as a resource for critical materials. *Nat. Rev. Earth Environ.* **2020**, *1*, 158–169. [CrossRef]
2. Ren, J.B.; Deng, Y.N.; Lai, P.X.; He, G.W.; Wang, F.L.; Yao, H.Q.; Deng, X.G.; Liu, Y.G. Geochemical characteristics and genesis of the polymetallic nodules in the Pacific survey area. *Earth Sci. Front.* **2021**, *28*, 412–425, (English Translation).
3. Wang, X.; Schloßmacher, U.; Wiens, M.; Schröder, H.C.; Müller, W.E. Biogenic origin of polymetallic nodules from the Clarion-Clipperton zone in the Eastern Pacific Ocean: Electron microscopic and EDX evidence. *Mar. Biotechnol.* **2009**, *11*, 99–108. [CrossRef]
4. Van, D.C.L. Inactive sulfide ecosystems in the deep sea: A review. *Front. Mar. Sci.* **2019**, *6*, 461.
5. Khripounoff, A.; Caprais, J.C.; Crassous, P.; Etoubleau, J. Geochemical and biological recovery of the disturbed seafloor in polymetallic nodule fields of the Clipperton-Clarion Fracture Zone (CCFZ) at 5000 m depth. *Limnol. Oceanogr.* **2006**, *51*, 2033–2041. [CrossRef]
6. Yaqoob, A.A.; Ahmad, A.; Alshammari, M.B. Advanced Technologies for Wastewater Treatment. *Green Chem. Sustain. Water Purif.* **2023**, *1*, 179–202.
7. Kang, B.; Zha, F.; Li, H.; Xu, L.; Sun, X.; Lu, Z. Bio-mediated method for immobilizing copper tailings sand contaminated with multiple heavy metals. *Crystals* **2022**, *12*, 522. [CrossRef]

8.   Chuo, S.C.; Mohamed, S.F.; Mohd Setapar, S.H.; Ahmad, A.; Jawaid, M.; Wani, W.A.; Yaqoob, A.A.; Mohamad Ibrahim, M.N. Insights into the current trends in the utilization of bacteria for microbially induced calcium carbonate Precipitation. *Materials* **2020**, *13*, 4993. [CrossRef]

9.   Khanjani, M.; Westenberg, D.J.; Kumar, A.; Ma, H. Tuning polymorphs and morphology of microbially induced calcium carbonate: Controlling factors and underlying mechanisms. *ACS Omega* **2021**, *6*, 11988–12003. [CrossRef]

10.   Xue, Z.F.; Cheng, W.C.; Wang, L.; Hu, W. Effects of bacterial inoculation and calcium source on microbial-induced carbonate precipitation for lead remediation. *J. Hazard. Mater.* **2022**, *426*, 128090. [CrossRef]

11.   Liu, Y.; Ali, A.; Su, J.F.; Li, K.; Hu, R.Z.; Wang, Z. Microbial-induced calcium carbonate precipitation: Influencing factors, nucleation pathways, and application in waste water remediation. *Sci. Total Environ.* **2023**, *860*, 160439. [CrossRef] [PubMed]

12.   Dewi, A.K.; Chen, T.H.; Lin, P.Y.; Sharma, R.K.; Huang, Y.H.; Lu, C.M.; Lu, C.K. Microbial-Induced Manganese Carbonate ($MnCO_3$) Precipitation for Heavy Metal Removal from Water. *SSRN Electron. J.* **2022**. [CrossRef]

13.   Xu, X.W.; Wu, Y.H.; Wang, C.S.; Wang, X.G.; Oren, A.; Wu, M. *Croceicoccus marinus* gen. nov., sp. nov., a yellow-pigmented bacterium from deep-sea sediment, and emended description of the family *Erythrobacteraceae*. *Int. J. Syst. Evol. Microbiol.* **2009**, *59*, 2247–2253. [CrossRef] [PubMed]

14.   Huang, Y.; Zeng, Y.; Feng, H.; Wu, Y.; Xu, X. *Croceicoccus naphthovorans* sp. nov., a polycyclic aromatic hydrocarbons-degrading and acylhomoserine-lactone-producing bacterium isolated from marine biofilm, and emended description of the genus *Croceicoccus*. *Int. J. Syst. Evol. Microbiol.* **2015**, *65*, 1531–1536. [CrossRef]

15.   Wu, Y.H.; Li, G.Y.; Jian, S.L.; Cheng, H.; Huo, Y.Y.; Wang, C.S.; Shao, Z.Z.; Xu, X.W. *Croceicoccus pelagius* sp. nov. and *Croceicoccus mobilis* sp. nov., isolated from marine environments. *Int. J. Syst. Evol. Microbiol.* **2016**, *66*, 4506–4511. [CrossRef]

16.   Shen, Y.; Li, Z.; Huo, Y.Y.; Bao, L.; Gao, B.; Xiao, P.; Hu, X.; Xu, X.W.; Li, J. Structural and functional insights into CmGH1, a novel GH39 family *β*-glucosidase from deep-sea bacterium. *Front. Microbiol.* **2019**, *10*, 2922. [CrossRef]

17.   Wu, Y.H.; Cheng, H.; Huo, Y.Y.; Xu, L.; Liu, Q.; Wang, C.S.; Xu, X.W. Complete genome sequence of esterase-producing bacterium *Croceicoccus marinus* E4A9[T]. *Stand. Genom. Sci.* **2017**, *12*, 88. [CrossRef]

18.   Huang, Y.; Wang, Y.; Feng, H.; Wang, J.; Yang, X.; Wang, Z. Genome-guided identification and characterization of bacteria for simultaneous degradation of polycyclic aromatic hydrocarbons and resistance to hexavalent chromium. *Int. Biodeter. Biodegr.* **2019**, *138*, 78–86. [CrossRef]

19.   Mbani, B.; Greinert, J. Analysis-ready optical underwater images of manganese-nodule covered seafloor of the Clarion-Clipperton Zone. *Sci. Data* **2023**, *10*, 316. [CrossRef]

20.   Sheng, M.; Peng, D.; Luo, S.; Ni, T.; Luo, H.; Zhang, R.; Wen, Y.; Xu, H. Micro-dynamic process of cadmium removal by microbial induced carbonate precipitation. *Environ. Pollut.* **2022**, *308*, 119585. [CrossRef]

21.   Sinegani, A.A.S.; Younessi, N. Antibiotic resistance of bacteria isolated from heavy metal-polluted soils with different land uses. *J. Glob. Antimicrob. Resist.* **2017**, *10*, 247–255. [CrossRef]

22.   Freeman, D.J.; Falkiner, F.R.; Keane, C.T. New method for detecting slime production by coagulase negative staphylococci. *J. Clin. Pathol.* **1989**, *42*, 872–874. [CrossRef] [PubMed]

23.   Hassan, A.; Usman, J.; Kaleem, F.; Omair, M.; Khalid, A.; Iqbal, M. Evaluation of different detection methods of biofilm formation in the clinical isolates. *J. Infect. Dis.* **2011**, *15*, 305–311.

24.   Dong, X.Z.; Cai, M.Y. *Determinative Manual for Routine Bacteriology*; Scientific Press: Beijing, China, 2001; (English Translation).

25.   Hildebrand, D.C.; Palleroni, N.J.; Hendson, M.; Toth, J.; Johnson, J.L. *Pseudomonas flavescens* sp. nov., isolated from walnut blight cankers. *Int. J. Syst. Evol. Microbiol.* **1994**, *44*, 410–415. [CrossRef] [PubMed]

26.   Farmer, J.J., III; Janda, J.M.; Brenner, F.W.; Cameron, D.N.; Birkhead, K.M. Genus I. Vibrio Pacini 1854, 411[AL]. In *Bergey's Manual of Systematic Bacteriology, the Proteobacteria, Part B, the Gammaproteobacteria*, 2nd ed.; Garrity, G.M., Brenner, D.J., Krieg, N.R., Staley, J.T., Eds.; Springer: New York, NY, USA, 2005; Volume 2, pp. 494–546.

27.   Leifson, E.J. Determination of carbohydrate metabolism of marine bacteria. *J. Bacteriol.* **1963**, *85*, 1183. [CrossRef] [PubMed]

28.   Park, Y.D.; Baik, K.S.; Yi, H.; Bae, K.S.; Chun, J. *Pseudoalteromonas byunsanensis* sp. nov., isolated from tidal flat sediment in Korea. *Int. J. Syst. Evol. Microbiol.* **2005**, *55*, 2519–2523. [CrossRef]

29.   Wu, Y.H.; Xu, L.; Zhou, P.; Wang, C.S.; Oren, A.; Xu, X.W. *Brevirhabdus pacifica* gen. nov., sp. nov., isolated from deep-sea sediment in a hydrothermal vent field. *Int. J. Syst. Evol. Microbiol.* **2015**, *65*, 3645–3651. [CrossRef]

30.   Komagata, K.; Suzuki, K.I. 4 Lipid and cell-wall analysis in bacterial systematics. *Method Microbiol.* **1988**, *19*, 161–207.

31.   Minnikin, D.E.; O'donnell, A.G.; Goodfellow, M.; Alderson, G.; Athalye, M.; Schaal, A.; Parlett, J.H. An integrated procedure for the extraction of bacterial isoprenoid quinones and polar lipids. *J. Microbiol. Methods* **1984**, *2*, 233–241. [CrossRef]

32.   Fang, M.X.; Zhang, W.W.; Zhang, Y.Z.; Tan, H.Q.; Zhang, X.Q.; Wu, M.; Zhu, X.F. *Brassicibacter mesophilus* gen. nov., sp. nov., a strictly anaerobic bacterium isolated from food industry wastewater. *Int. J. Syst. Evol. Microbiol.* **2012**, *62*, 3018–3023. [CrossRef]

33.   Lagesen, K.; Hallin, P.; Rødland, E.A.; Stærfeldt, H.H.; Rognes, T.; Ussery, D.W. RNAmmer: Consistent and rapid annotation of ribosomal RNA genes. *Nucleic Acids Res.* **2007**, *35*, 3100–3108. [CrossRef]

34.   Aziz, R.K.; Bartels, D.; Best, A.A.; DeJongh, M.; Disz, T.; Edwards, R.A.; Formsma, K. The RAST Server: Rapid annotations using subsystems technology. *BMC Genom.* **2008**, *9*, 75. [CrossRef] [PubMed]

35.   Kanehisa, M.; Goto, S. KEGG: Kyoto encyclopedia of genes and genomes. *Nucleic Acids Res.* **2000**, *28*, 27–30. [CrossRef]

36.   Yoon, S.H.; Ha, S.M.; Kwon, S.; Lim, J.; Kim, Y.; Seo, H.; Chun, J. Introducing EzBioCloud: A taxonomically united database of 16S rRNA gene sequences and whole-genome assemblies. *Int. J. Syst. Evol. Microbiol.* **2017**, *67*, 1613–1617. [CrossRef] [PubMed]

37. Tamura, K.; Stecher, G.; Kumar, S. MEGA11: Molecular evolutionary genetics analysis version 11. *Mol. Biol. Evol.* **2021**, *38*, 3022–3027. [CrossRef] [PubMed]

38. Seemann, T. Prokka: Rapid prokaryotic genome annotation. *Bioinformatics* **2014**, *30*, 2068–2069. [CrossRef]

39. Lechner, M.; Hernandez-Rosales, M.; Doerr, D.; Wieseke, N.; Thévenin, A.; Stoye, J.; Hartmann, R.K.; Prohaska, S.J.; Stadler, P.F. Orthology detection combining clustering and synteny for very large datasets. *PLoS ONE* **2014**, *9*, e105015. [CrossRef]

40. Katoh, K.; Standley, D.M. MAFFT multiple sequence alignment software version 7: Improvements in performance and usability. *Mol. Biol. Evol.* **2013**, *30*, 772–780. [CrossRef]

41. Capella-Gutiérrez, S.; Silla-Martínez, J.M.; Gabaldón, T. trimAl: A tool for automated alignment trimming in large-scale phylogenetic analyses. *Bioinformatics* **2009**, *25*, 1972–1973. [CrossRef]

42. Nguyen, L.T.; Schmidt, H.A.; Von, H.A.; Minh, B.Q. IQ-TREE: A fast and effective stochastic algorithm for estimating maximum-likelihood phylogenies. *Mol. Biol. Evol.* **2015**, *32*, 268–274. [CrossRef]

43. Yoon, S.H.; Ha, S.M.; Lim, J.; Kwon, S.; Chun, J. A large-scale evaluation of algorithms to calculate average nucleotide identity. *Antonie Van Leeuwenhoek* **2017**, *110*, 1281–1286. [CrossRef]

44. Meier-Kolthoff, J.P.; Auch, A.F.; Klenk, H.P.; Göker, M. Genome sequence-based species delimitation with confidence intervals and improved distance functions. *BMC Bioinform.* **2013**, *14*, 60. [CrossRef] [PubMed]

45. Li, L.; Stoeckert, C.J.; Roos, D.S. OrthoMCL: Identification of ortholog groups for eukaryotic genomes. *Genome Res.* **2003**, *13*, 2178–2189. [CrossRef] [PubMed]

46. Galperin, M.Y.; Wolf, Y.I.; Makarova, K.S.; Vera, A.R.; Landsman, D.; Koonin, E.V. COG database update: Focus on microbial diversity, model organisms, and widespread pathogens. *Nucleic Acids Res.* **2021**, *49*, D274–D281. [CrossRef]

47. Hatayama, K.J.G.J. Manganese carbonate precipitation induced by calcite-forming bacteria. *Geomicrobiol. J.* **2020**, *37*, 603–609. [CrossRef]

48. Zhu, Y.; Mam, N.; Jin, W.; Wu, S.; Sun, C. Genomic and transcriptomic insights into calcium carbonate biomineralization by marine actinobacterium *Brevibacterium linens* BS258. *Front. Microbiol.* **2017**, *8*, 602. [CrossRef] [PubMed]

49. Zhang, W.; Ju, Y.; Zong, Y.; Qi, H.; Zhao, K. In situ real-time study on dynamics of microbially induced calcium carbonate precipitation at a single-cell level. *Environ. Sci. Technol.* **2018**, *52*, 9266–9276. [CrossRef]

50. Xu, L.; Sun, C.; Fang, C.; Oren, A.; Xu, X.W. Genomic-based taxonomic classification of the family *Erythrobacteraceae*. *Int. J. Syst. Evol. Microbiol.* **2020**, *70*, 4470. [CrossRef]

51. Richter, M.; Rosselló-Móra, R. Shifting the genomic gold standard for the prokaryotic species definition. *Proc. Natl. Acad. Sci. USA* **2009**, *106*, 19126–19131. [CrossRef]

52. Wayne, L.G.; Brenner, D.J.; Colwell, R.R.; Grimont, P.A.D.; Kandler, O.; Krichevsky, M.I. Report of the ad hoc committee on reconciliation of approaches to bacterial systematics. *Int. J. Syst. Evol. Microbiol.* **1987**, *37*, 463–464. [CrossRef]

53. Danese, P.N.; Pratt, L.A.; Dove, S.L.; Kolter, R. The outer membrane protein, antigen 43, mediates cell-to-cell interactions within *Escherichia coli* biofilms. *Mol. Microbiol.* **2000**, *37*, 424–432. [CrossRef] [PubMed]

54. Prigent-Combaret, C.; Prensier, G.; Le, T.T.T.; Vidal, O.; Lejeune, P.; Dorel, C. Developmental pathway for biofilm formation in curli-producing *Escherichia coli* strains: Role of flagella, curli and colanic acid. *Environ. Microbiol.* **2000**, *2*, 450–464. [CrossRef] [PubMed]

55. Reisner, A.; Haagensen, J.A.; Schembri, M.A.; Zechner, E.L.; Molin, S. Development and maturation of *Escherichia coli* K-12 biofilms. *Mol. Microbiol.* **2003**, *48*, 933–946. [CrossRef]

56. Luo, G.; Huang, L.; Su, Y.; Qin, Y.; Xu, X.; Zhao, L.; Yan, Q. *flrA*, *flrB* and *flrC* regulate adhesion by controlling the expression of critical virulence genes in *Vibrio alginolyticus*. *Emerg. Microbes. Infect.* **2016**, *5*, e85. [CrossRef] [PubMed]

57. Drummelsmith, J.; Whitfield, C. Translocation of group 1 capsular polysaccharide to the surface of *Escherichia coli* requires a multimeric complex in the outer membrane. *EMBO J.* **2000**, *19*, 57–66. [CrossRef]

58. Nesper, J.; Hill, C.M.; Paiment, A.; Harauz, G.; Beis, K.; Naismith, J.H.; Whitfield, C. Translocation of group 1 capsular polysaccharide in *Escherichia coli* serotype K30: Structural and functional analysis of the outer membrane lipoprotein Wza. *J. Biol. Chem.* **2003**, *278*, 49763–49772. [CrossRef]

59. Whitfield, C.; Paiment, A. Biosynthesis and assembly of group 1 capsular polysaccharides in *Escherichia coli* and related extracellular polysaccharides in other bacteria. *Carbohydr. Res.* **2003**, *338*, 2491–2502. [CrossRef]

60. Beis, K.; Collins, R.F.; Ford, R.C.; Kamis, A.B.; Whitfield, C.; Naismith, J.H. Three-dimensional structure of Wza, the protein required for translocation of group 1 capsular polysaccharide across the outer membrane of *Escherichia coli*. *J. Biol. Chem.* **2004**, *279*, 28227–28232. [CrossRef]

61. Reid, A.N.; Whitfield, C. Functional analysis of conserved gene products involved in assembly of *Escherichia coli* capsules and exopolysaccharides: Evidence for molecular recognition between Wza and Wzc for colanic acid biosynthesis. *J. Bacteriol.* **2005**, *187*, 5470–5481. [CrossRef]

62. Yong, Y.C.; Zhong, J.J. Impacts of quorum sensing on microbial metabolism and human health. *Trends Biotechnol.* **2013**, *131*, 25–61.

63. Monteiro, C.; Papenfort, K.; Hentrich, K.; Ahmad, I.; Le, G.S.; Reimann, R.; Grantcharova, N.; Römling, U. Hfq and Hfq-dependent small RNAs are major contributors to multicellular development in *Salmonella enterica* serovar Typhimurium. *RNA Biol.* **2012**, *9*, 489–502. [CrossRef] [PubMed]

64. Fazli, M.; Rybtke, M.; Steiner, E.; Weidel, E.; Berthelsen, J.; Groizeleau, J.; Bin, W.; Zhi, B.Z. Regulation of *Burkholderia cenocepacia* biofilm formation by RpoN and the c-di-GMP effector BerB. *Microbiol. Open* **2017**, *6*, e00480. [CrossRef] [PubMed]

65. Hausrath, A.C.; Ramirez, N.A.; Ly, A.T.; McEvoy, M.M. The bacterial copper resistance protein CopG contains a cysteine-bridged tetranuclear copper cluster. *J. Biol. Chem.* **2020**, *295*, 11364–11376. [CrossRef] [PubMed]

66. Butterfield, C.N.; Soldatova, A.V.; Lee, S.W.; Spiro, T.G.; Tebo, B.M. Mn(II, III) oxidation and MnO_2 mineralization by an expressed bacterial multicopper oxidase. *Proc. Natl. Acad. Sci. USA* **2013**, *110*, 11731–11735. [CrossRef]

67. Kaur, K.; Sharma, A.; Capalash, N.; Sharma, P. Multicopper oxidases: Biocatalysts in microbial pathogenesis and stress management. *Microbiol. Res.* **2019**, *222*, 1–13. [CrossRef]

68. Geszvain, K.; Smesrud, L.; Tebo, B.M. Identification of a third Mn(II) oxidase enzyme in *Pseudomonas putida* GB-1. *Appl. Environ. Microb.* **2016**, *82*, 3774–3782. [CrossRef]

69. Zhou, H.; Fu, C. Manganese-oxidizing microbes and biogenic manganese oxides: Characterization, Mn (II) oxidation mechanism and environmental relevance. *Rev. Environ. Sci. Bio* **2020**, *19*, 489–507. [CrossRef]

70. Wu, H.X.; Lai, P.Y.; Lee, O.O.; Zhou, X.J.; Miao, L.; Wang, H.; Qian, P.Y. *Erythrobacter pelagi* sp. nov., a member of the family *Erythrobacteraceae* isolated from the Red Sea. *Int. J. Syst. Evol. Microbiol.* **2012**, *62 Pt 6*, 1348–1353. [CrossRef]

71. Pal, C.; Bengtsson-Palme, J.; Rensing, C.; Kristiansson, E.; Larsson, D.J. BacMet: Antibacterial biocide and metal resistance genes database. *Nucleic Acids Res.* **2014**, *42*, D737–D743. [CrossRef]

72. Yutin, N.; Suzuki, M.T.; Teeling, H.; Weber, M.; Venter, J.C.; Rusch, D.B.; Béjà, O. Assessing diversity and biogeography of aerobic anoxygenic phototrophic bacteria in surface waters of the Atlantic and Pacific Oceans using the Global Ocean Sampling expedition metagenomes. *Environ. Microbiol.* **2007**, *9*, 1464–1475. [CrossRef]

73. Mukhopadhyay, R.; Rosen, B.P. Arsenate reductases in prokaryotes and eukaryotes. *Environ. Health Perspect.* **2002**, *110*, 745–748. [CrossRef] [PubMed]

74. Hou, Y.; Cheng, K.; Li, Z.; Ma, X.; Wei, Y.; Zhang, L.; Wang, Y. Biosorption of cadmium and manganese using free cells of *Klebsiella* sp. isolated from waste water. *PLoS ONE* **2015**, *10*, e0140962. [CrossRef]

75. Dey, S.; Paul, A.K. Assessment of heavy metal tolerance and hexavalent chromium reducing potential of *Corynebacterium paurometabolum* SKPD 1204 isolated from chromite mine seepage. *AIMS Bioeng.* **2016**, *3*, 337–351. [CrossRef]

76. Xu, L.; Xu, X.W.; Meng, F.X.; Huo, Y.Y.; Oren, A.; Yang, J.Y.; Wang, C.S. *Halomonas zincidurans* sp. nov., a heavy-metal-tolerant bacterium isolated from the deep-sea environment. *Int. J. Syst. Evol. Microbiol.* **2013**, *63*, 4230–4236. [CrossRef]

77. Wang, X.; Lin, D.; Jing, X.; Zhu, S.; Yang, J.; Chen, J. Complete genome sequence of the highly Mn(II) tolerant *Staphylococcus* sp. AntiMn-1 isolated from deep-sea sediment in the Clarion-Clipperton Zone. *J. Biotechnol.* **2018**, *266*, 34–38. [CrossRef] [PubMed]

78. Gillard, B.; Chatzievangelou, D.; Thomsen, L.; Ullrich, M.S. Heavy-metal-resistant microorganisms in deep-sea sediments disturbed by mining activity: An application toward the development of experimental in vitro systems. *Front. Mar. Sci.* **2019**, *6*, 462. [CrossRef]

79. Wu, Y.H.; Fang, C.; Zhou, P.; Wang, C.S.; Xu, X.W. Complete genome sequence of a heavy metal resistant bacterium *Maribacter cobaltidurans* B1^T, isolated from the deep-sea sediment of the South Atlantic Ocean. *Mar. Genom.* **2018**, *39*, 19–21. [CrossRef]

80. Wu, Y.H.; Cheng, H.; Zhou, P.; Huo, Y.Y.; Wang, C.S.; Xu, X.W. Complete genome sequence of the heavy metal resistant bacterium *Altererythrobacter atlanticus* 26DY36^T, isolated from deep-sea sediment of the North Atlantic Mid-ocean ridge. *Mar. Genom.* **2015**, *24*, 289–292. [CrossRef]

81. Wang, W.; Shao, Z.; Liu, Y.; Wang, G. Removal of multi-heavy metals using biogenic manganese oxides generated by a deep-sea sedimentary bacterium–*Brachybacterium* sp. strain Mn32. *Microbiol. Res.* **2009**, *155*, 1989–1996. [CrossRef]

82. Du, R.; Gao, D.; Wang, Y.; Liu, L.; Cheng, J.; Liu, J.; Zhang, X.H.; Yu, M. Heterotrophic sulfur oxidation of *Halomonas titanicae* SOB56 and its habitat adaptation to the hydrothermal environment. *Front. Microbiol.* **2022**, *13*, 888833. [CrossRef]

83. Flemming, H.C.; Wingender, J.; Szewzyk, U.; Steinberg, P.; Rice, S.A.; Kjelleberg, S. Biofilms: An emergent form of bacterial life. *Nat. Rev. Microbiol.* **2016**, *14*, 563–575. [CrossRef]

84. Yin, K.; Wang, Q.; Lv, M.; Chen, L. Microorganism remediation strategies towards heavy metals. *Chem. Eng. J.* **2019**, *360*, 1553–1563. [CrossRef]

85. Radisky, D.; Kaplan, J. Regulation of transition metal transport across the yeast plasma membrane. *J. Biol. Chem.* **1999**, *274*, 4481–4484. [CrossRef] [PubMed]

86. Abdel-Ghany, S.E.; Muller-Moule, P.; Niyogi, K.K.; Pilon, M.; Shikanai, T. Two P-type ATPases are required for copper delivery in *Arabidopsis thaliana* chloroplasts. *Plant Cell* **2005**, *17*, 1233–1251. [CrossRef] [PubMed]

87. Frankel, R.B.; Bazylinski, D.A. Bazylinski, and geochemistry, Biologically induced mineralization by bacteria. *Rev. Mineral. Geochem.* **2003**, *54*, 95–114. [CrossRef]

88. Ercole, C.; Bozzelli, P.; Altieri, F.; Cacchio, P.; Del, G.M. Calcium carbonate mineralization: Involvement of extracellular polymeric materials isolated from calcifying bacteria. *Microsc. Microanal.* **2012**, *18*, 829–839. [CrossRef] [PubMed]

89. Decho, A.W.; Gutierrez, T. Microbial extracellular polymeric substances (EPSs) in ocean systems. *Front. Microbiol.* **2017**, *8*, 922. [CrossRef] [PubMed]

90. Picard, A.; Gartman, A.; Clarke, D.R.; Girguis, P.R. Sulfate-reducing bacteria influence the nucleation and growth of mackinawite and greigite. *Geochim. Cosmochim. Acta* **2018**, *220*, 367–384. [CrossRef]

91. Achal, V.; Pan, X. Characterization of urease and carbonic anhydrase producing bacteria and their role in calcite precipitation. *Curr. Microbiol.* **2011**, *62*, 894–902. [CrossRef]

92. Teng, Z.; Shao, W.; Zhang, K.; Huo, Y.; Zhu, J.; Li, M. Pb biosorption by *Leclercia adecarboxylata*: Protective and immobilized mechanisms of extracellular polymeric substances. *Chem. Eng. J.* **2019**, *375*, 122113. [CrossRef]
93. Han, L.; Li, J.; Xue, Q.; Chen, Z.; Zhou, Y.; Poon, C.S. Bacterial-induced mineralization (BIM) for soil solidification and heavy metal stabilization: A critical review. *Sci. Total Environ.* **2020**, *746*, 140967. [CrossRef] [PubMed]